Evaluating and Extending the Arctic Monitoring and Assessment Programme (AMAP) Climate Emulator

by

Victoria Spada

Supervisors: Paul Kushner and Knut von Salzen

April 2023

B.A.Sc. Thesis

Division of Engineering Science
UNIVERSITY OF TORONTO

Evaluating and Extending the Arctic Monitoring and Assessment Programme (AMAP) Climate Emulator

Supervisors: Paul Kushner and Knut von Salzen

Student: Victoria Spada

April 2023

Abstract

Short-lived climate forcers can have a great impact on human health and climate change, particularly in the Arctic. The AMAP climate emulator is a simple mass and energy balance model that can be used to quickly produce projections of global surface air temperature for four latitude bands. It has a relatively low equilibrium climate sensitivity (before scaling) compared to recent, state-of-the art ESMs, and was shown to underestimate Arctic amplification when compared to ESMs from CMIP6. The limitations and potential of the emulator were explored. In an area-weighted rescaling of the RTP coefficients used by the AMAP emulator, an increase in RTP_{ARC} between 25% and 50% was found to be appropriate for the emulator to better represent Arctic amplification, though the CMIP6 ensemble results used for comparison produced high uncertainties. The equilibrium climate sensitivity is an important parameter to consider when modifying the RTP coefficients. Natural emissions of CH_4 were additionally incorporated into the emulator as a positive linear feedback from Arctic temperature to account for the potential increase in anaerobic respiration as a natural CH_4 source. The emulator was run with a CH_4 natural emissions feedback loop of variable strength dependent on Arctic temperature perturbations to investigate the potential of this addition to the model and its impacts on how different scenarios affect regional and global temperatures.

Acknowledgements

I would like to express my deepest gratitude to Prof. Paul Kushner and Dr. Knut von Salzen for their supervision, mentorship, and support while conducting this study, for this endeavor would not have been possible without their guidance. Many thanks to Dr. Michael Sigmund for his support and insight throughout the project. I had the pleasure of working with the Kushner Group at the University of Toronto Department of Physics, and extend my thanks to them as well, for their supportive impact.

Contents

1 Introduction **1**

2 Background **2**

2.1 Climate Change and Short-lived Climate Forcers 2

2.1.1 Methane 2

2.1.2 Ozone 2

2.1.3 Sulfate Aerosols 3

2.1.4 Black Carbon and Organic Carbon 3

2.1.5 Impacts of SLCFs 3

2.2 Evaluating ESMs and Climate Emulators 3

2.3 A Survey of Climate Emulators 5

2.4 The AMAP Air Quality and Climate Emulator 7

2.5 Evaluating the AMAP Emulator and other Emulators 11

2.6 Synthesis 12

3 Methods **13**

3.1 Evaluating the AMAP Emulator 13

3.1.1 Extending and Existing Study 13

3.1.2 Comparing the AMAP Emulator Results with a Larger CMIP6 Ensemble . 14

3.2 Tweaking RTP Coefficients 15

3.2.1 Processing the Emulator Results and CMIP6 Results 16

3.3 Incorporating a Feedback Loop for Methane Emissions 17

4 Results and Discussion **17**

4.1 Evaluating the AMAP Emulator 17

4.2 Tweaking RTP Coefficients 29

4.3 Incorporating a Feedback Loop for Methane Emissions 30

5 Conclusion **30**

List of Figures

1 Time series of the regional and global surface air temperature anomalies projected by the AMAP emulator, for four SSPs, relative to a reference period of 1995-2014. The standard deviation of the temperatures realized for each year was taken as the SAT anomaly uncertainty for that year. 19

2 Time series of the regional and global surface air temperature anomalies projected by the AMAP emulator, for four SSPs, relative to a reference period of 1995-2014. The standard deviation of the temperatures realized for each year was taken as the SAT anomaly uncertainty for that year. 20

3 Projected global and Arctic mean surface air temperature changes in 2050. The net temperature changes projected by the AMAP emulator are plotted as circles, the CMIP6 multi-model median values as diamonds. The 5–95% confidence intervals ($\pm 1.64\sigma$), resulting from uncertainties in all simulated processes, are shown as black error bars. Confidence ranges due to radiative forcing uncertainty in the AMAP emulator are shown as rectangles. Color bars refer to the forced temperature change from the individual air pollutant and greenhouse gas species, based on AMAP emulator simulations. Warming relative to preindustrial conditions is also indicated (grey font, with 1.5 and 2 °C thresholds indicated by dashed lines in (a)). 22

4 Same as Figure 3, but for the year 2030. 23

5 Time series of the regional amplifications for the 4 regions projected by the AMAP emulator, for SSP1-2.6, SSP2-4.5, SSP3-7.0, and SSP5-8.5. The regional amplification for each year is represented as the ratio of the average regional SAT anomaly across the ensemble (with reference to the period of 1995-2014) to the average global SAT anomaly. The error bars represent the propagated uncertainty of the two mean SAT anomalies in the dividend (regional and global). 24

6 Same as Figure 5, but for the CMIP6 ensemble. Error bars are neglected in this figure to focus on the variation across the SSPs. A version of this plot with error bars is shown in Appendix C, Figure 13. 25

7 Results of RMA fitting of global versus regional SAT anomalies from the large CMIP6 ensemble for four SSPs, along with the resulting slopes m from the fits . . 27
8 Results of RMA fitting of global versus regional SAT anomalies from AMAP ensemble for four SSPs, along with the resulting slopes m from the fits. 28
9 Time series of the regional surface air temperature anomalies projected by the AMAP emulator with tweaked RTP coefficients (different δ settings), relative to a reference period of 1995-2014. The standard deviation of the temperatures realized for each year was taken as the SAT anomaly uncertainty for that year. These results are shown for SSP5-8.5, and are plotted alongside the projected surface air temperature anomalies from the CMIP6 ensemble. 31
10 Regional amplification projected by the AMAP emulator for different δ settings, for SSP5-8.5. The uncertainty of these time series shown as filled in colour, and are standard deviation of the temperatures from the ensemble was taken as the temperature uncertainty for each year. This uncertainty was propagated with the uncertainty from the mean temperature over the reference period of 1995-2014. The corresponding results from the CMIP6 ensemble are shown for comparison, but error bars are neglected due to their large relative size. The uncertainties for these CMIP6 ensemble time series are shown in Figure 13 in Appendix C. 32
11 Results of RMA fitting of global versus regional SAT anomalies for four AMAP emulator tweakings, $\delta = \{0.00, 0.10, 0.25, 0.50\}$ and the large CMIP6 ensemble, for SSP5-8.5, along with the resulting slope m from the fits.. 33
12 Natural emissions of CH_4 as a function of time and the Arctic temperature perturbations projected by the modified AMAP emulator, for SSP5-8.5. 34
13 Same as Figure 6, but with added error bars shown through shaded colour for each of the SSPs. The standard deviation of the temperatures from the ensemble was taken as the temperature uncertainty for each year. The error bars are the propagated uncertainty of the two mean SAT anomalies in the dividend (regional and global). 45

14 Global surface temperature anomalies relative to 1995-2014 projected for 2050 by CMIP6 ensemble and regional amplifications for the Arctic, Northern Hemisphere midlatitudes, the tropics, and the Southern Hemisphere in the year Amplification. For each of the four SSPs, the coloured points represent the global anomaly from an individual realization from the CMIP6 ensemble (upper left) or the ratio of a regional surface temperature anomaly to the global anomaly for a particular region (upper middle and right, bottom). The black bullets represent the ensemble average regional surface temperature anomaly divided by the ensemble global surface temperature anomaly for 2050. 46

15 Same as Figure 14, but for an ensemble of 24 realizations of AMAP emulator on its default settings ($\delta = 0.00$). 47

List of Tables

1 Survey of recent climate emulators. 6

2 Time scales of CH_4 loss processes accounted for in its atmospheric lifetime in the AMAP emulator, following [7], [50], [51], and [52]. 10

3 Mean relative and absolute differences corresponding to Figures 4 and 3, across the five SSPs. 21

4 Mean of estimated slopes of global versus regional surface temperature anomalies [°C / °C], across SSP1-2.6, SSP2-4.5, SSP3-7.0, and SSP5-8.5. The uncertainty of these average slopes were taken by propagating the uncertainties of the individual slopes. 27

5 Mean resulting slopes of global versus regional SAT anomalies [°C / °C] for SSP5-8.5. The uncertainty of these average slopes were taken by propagating the uncertainties of the individual slopes. 30

6 Climate models included in the CMIP6 ensemble for each of the SSPs shown in Figures 3 and 4. 43

7 RTP coefficients k_{lm} for an AMAP emulator settings of $\delta \in \{\, 0.00, 0.10, 0.25, 0.50\}$, rounded to 3 significant figures for the modified coefficient versions. The default coefficients ($\delta = 0.00$) are shown with two decimal places because that is the default setting of the emulator. 44

8 This table presents the regional amplifications, taken as the average regional surface air temperature anomaly to the global anomaly. for SSP5-8.5 for the large CMIP6 ensemble at the AMAP emulator in its default setting ($\text{AMAP}_{\delta=0.00}$) and tweaked settings ($\text{AMAP}_{\delta=0.10}$, $\text{AMAP}_{\delta=0.25}$, $\text{AMAP}_{\delta=0.50}$). The regional amplifications are shown for the years 2030 and 2050. 48

1 Introduction

Computational Earth System Models (ESMs) are used to simulate projected warming, climate change, and air quality scenarios. However, they are computationally expensive, which may not be suitable for climate and air quality assessments in which the effects of multiple pollutants are considered. Climate emulators and air quality source-receptor models employ analytic relationships between emissions, concentrations, and radiative forcing, using inexpensive models that highly approximate, parameterize, and even linearize the impacts of Earth's complex physical and chemical processes on climate [1], [2]. Short-lived climate forcers (SLCFs) are a group of greenhouse gases (GHGs) and other pollutants that have relatively short atmospheric lifetimes compared to carbon dioxide (CO_2) and can greatly impact climate change and air quality [3]. Due to their short lifetimes and trace amounts, which result in high uncertainties even in ESMs, emulators are a computationally inexpensive and effective tool for SLCF science in support of climate and air quality policy development [1], [3], [4].

The Arctic Monitoring and Assessment Programme (AMAP) Air Quality and Climate Emulator (hereafter referred to as the AMAP emulator) uses a greatly simplified ESM to predict changes in air quality and climate in four regions based on regional anthropogenic emissions of air pollutants and GHGs, including SLCFs. The tool is new and has the potential for tuning, extension, and numerous applications in climate science and policy. However, the emulator has limitations [1].

One important limitation of the AMAP emulator relates to Arctic amplification, which refers to the enhancement of changes in surface temperature over the Arctic relative to lower latitudes [5]. The AMAP emulator has been found to underestimate Arctic amplification when compared to Coupled Model Intercomparison Project Phase 6 (CMIP6) ESMs [1], [6].

Additionally, methane (CH_4) is treated as a well-mixed GHG without spatial structure in radiative forcings or dependence on regional emission sources. Natural emissions of $CH4_4$ are set as a constant 202.0 Tg/year as suggested by [7]. Uncertainties in Arctic temperature projections resulting from uncertainties in natural CH_4 emissions are high because the emulator lacks an estimate of future natural emissions [1].

The purpose of this study is to better characterize and address the limitations of the AMAP emulator. The emulator's output was reviewed and evaluated, with a focus on analyzing and tuning

the climate output of the emulator in the Arctic for different emissions scenarios [8], [9].

2 Background

To provide background on this study, this literature review begins with a more in-depth introduction to SLCFs and their impacts on global climate change and health, and how they motivate climate emulation. Then, recent intercomparison studies of ESMs and Reduced Complexity Models (RCMs) are explored, and some state-of-the-art climate emulators are reviewed. The AMAP emulator is outlined in detail. Finally, results of studies involving the AMAP emulator that motivate the goals of the study are discussed.

2.1 Climate Change and Short-lived Climate Forcers

SLCFs can greatly contribute to global warming and impact air quality. Some of the key SLCFs are black carbon (BC), CH_4, organic carbon (OC), tropospheric ozone (O_3), and hydrofluorocarbons (HFCs). They are emitted by a variety of sources and have a wide range of climate impacts [3], [4], [10].

2.1.1 Methane

CH_4 is a GHG with a high radiative efficiency. Since it has an atmospheric lifetime of about 12 years, which is relatively high compared to other SLCFs, which can have atmospheric lifetimes on the order of days or weeks, it is sometimes considered a well-mixed GHG as opposed to a SLCF. Still, this atmospheric lifetime is quite small compared to that of CO_2, which is on the order of hundreds or a thousand years. CH_4 affects air quality as a precursor to tropospheric O_3. It also acts a precursor to stratospheric water vapour, another GHG [4], [10], [11], [12], [13].

2.1.2 Ozone

O_3 is an air pollutant and GHG that forms in the stratosphere when sunlight interacts with its precursor gases, such as CH_4, CO, non-CH_4 volatile organic compounds (NMVOCs) and nitrogen

oxides (NO_x) [4], [10]. Its atmospheric lifetime ranges from hours in urban areas to up to weeks or months in the upper troposphere [12].

2.1.3 Sulfate Aerosols

Sulfate (SO_4) aerosols form from sulfur compound emissions and account for much of PM2.5 (fine particles in the atmosphere with a diameter ≤ 2.5 μm). They efficiently scatter sunlight and increase the albedo of clouds, causing less solar radiation to reach Earth's surface. This results in cooling that counteracts the warming effects of other SLCFs and GHGs [4], [10]. This cooling impact is sometimes referred to as "masking" [4], [6]. The impacts of louds are an important source of uncertainty in climate modelling [14]. With globally declining levels of sulfate aerosols in the past three decades, the masking effect of these aerosols on global warming is diminishing, which enhances global and Arctic warming [3], [4], [15].

2.1.4 Black Carbon and Organic Carbon

BC and OC are also SLCFs that contribute to global warming and can degrade air quality. BC decreases the albedo of snow when deposited overtop it, and it is thus an important SLCF in Arctic climatology [3], [16], [17].

2.1.5 Impacts of SLCFs

In addition to combating global warming, reducing emissions of SLCFs can improve human health globally. Atmospheric O_3 and particulate matter have been linked with an increased risk for respiratory disease, premature death, and other adverse health outcomes [4], [18], [19], [20]. SLCFs can degrade air quality and contribute to climate change, and though these topics are often considered separately, there are strong links between them, as evidenced by recent studies [21], [22], [23].

2.2 Evaluating ESMs and Climate Emulators

In 2020, the Reduced Complexity Model Intercomparison Project (RCMIP) was launched to mirror CMIP (Coupled Model Intercomparison Project), a global project which examines and compares numerous cutting-edge comprehensive ESMs and Atmosphere-Ocean General Circulation

Model (AOGCMs) [2]. RCMIP uses scenario-based and idealized scenarios to study simulated global-mean temperature responses from various climate emulators, also called reduced complexity models (RCMs).

CMIP is an major project in the realm of climate modelling and climate change, as by evaluating and comparing the output for plausible emissions scenarios with cutting-edge ESMs, a better understanding of climate change can be attained and a benchmark for climate modelling can be set. The current generation of CMIP Phase 6 (CMIP6) ESMs was found to produce the greatest range of equilibrium climate sensitivity (ECS) values of any phase to date, ranging from 1.8 to 5.6 K, a range derived from 37 models [14], [24]. The ECS is a commonly used parameter in Earth system modelling that quantifies the global surface temperature response associated with doubling Earth's atmospheric CO_2 concentration [14].

RCMs are highly valuable for their low computational costs, high speed, and good estimation abilities, so the establishment of an ongoing comprehensive evaluation and assessment of RCMs is of interest. As of April 2023, two phases of RCMIP have been conducted, with a third phase currently in progress [2], [25].

Phase 1 of RCMIP defined its experiments with species concentrations to facilitate a direct comparison with CMIP experiments, which use Shared Socioeconomic Pathways (SSPs). SSPs are plausible scenarios of global anthropogenic development that would results in different challenges in mitigating climate change [26]. Specifically, there are five umbrella narratives for socioeconomic development: sustainable development (SSP1), middle-of-the-road development (SSP2), regional rivalry (SSP3), inequality (SSP4), and fossil-fueled development (SSP5). SSPs are widely used in climate modelling because they provide a point of comparison across climate models for range of outcomes for Earth's future.

The primary difference between the RCMIP and CMIP experiments is that RCMs often incorporate more anthropogenic driver species, such as all of the hydrofluorocarbon (HFC), fluorocarbon (PFC), and hydrochlorofluorocarbon (HCFC) species, and aerosols precursors [2].

In addition to valuable intercomparison, RCMIP enables comparisons with complex models by using similar, and some identical scenarios used in CMIP. Quantifying how much the simplifications in RCMs reduce their competence to replicate forcing and temperature responses from complex models is crucial to evaluating their utility. Phase 1 of RCMIP showed that RCMs were

able to capture the temperature responses of CMIP5 and CMIP6 models within a root mean-square error of 0.2 °C [2].

2.3 A Survey of Climate Emulators

While climate emulators are much simpler than comprehensive ESMs, they have been able to reproduce forced temperature trends simulated by ESMs within the uncertainty of the ESM simulations for many scenarios [1], [27], [28], [29], [30], [31] , [32]. Additionally, source-receptor models have been used to simulate the effects of numerous emissions scenarios on global air quality 1],[33],[34], [35],[36],[37].

The following is a survey of some recent climate emulators that were included in RCMIP Phase 1. Some key similarities and differences between these emulators, including the AMAP emulator, are shown in Table 1.

The OSCAR v2.2 emulator [32] is a climate emulator that models emissions with an impulse response, which is commonly used in climate emulators [2], [25], [31],[32], [38]. The climate model includes the oceanic and terrestrial carbon cycles to simulate atmospheric CO_2, tropospheric chemistry and natural wetlands to simulate atmospheric CH_4 and O_3, stratospheric chemistry to simulate NO and O_3, 37 halogenated compounds, dynamic surface albedo due to BC deposited on snow and land cover changes, and the resulting effects on aerosols. The forcing due to anthropogenic emissions incorporates CO_2 from burning fossil fuels and cement production, CH_4, NO, halogenated compounds, CO, NMVCs, SO2, NH_4, BC, and OC [32].

The FaIR v1.1 emulator an emissions-based climate emulator that also models emissions as an impulse response [31]. It has a global resolution and computes atmospheric concentrations of GHGs, outputting the resulting concentrations and effective radiative forcings (ERF) of these greenhouse gases, as well as aerosols, O_3 precursors and other agents. It includes a total of 13 forcing agents: CO_2, CH_4, N_2O, other GHGs, tropospheric O_3, stratospheric O_3, stratospheric water vapour, contrails, aerosols, BC on snow, land use change, and volcanic and solar activity.

The ERFs are used to calculate the global mean surface temperature change. The calculated change in temperature is then incorporated into a carbon cycle feedback, impacting the atmospheric lifetime of carbon dioxide [31].

Table 1: Survey of recent climate emulators.

Model	Spatial Resolution	Forcing Agents	Climate Response to Radiative Forcing
AMAP	4 latitude bands (60°N-90°N, 28°N-60°N, 28°S-28°S, and 90°S-28°S)	CH_4, OC, BC, sulfate, O_3, CO_2	Modified impulse response
FaIR v1.1	Global	CO_2, CH_4, N_2O, other GHGs, stratospheric and tropospheric O_3, stratospheric water vapour, contrails, aerosols, BC, land use change, and volcanic and solar activity	Modified impulse response
MAGICC	Hemispheric land/ocean	CO_2 (including terrestrial and ocean carbon cycles and athropogenic emissions), CH_4, NO, tropospheric aerosols, tropospheric and stratospheric O_3, and various halogenated gases	Atmospheric energy balance model with 50-layer upwelling diffusion- entrainment ocean
OSCAR v2.2	Global with regionalised carbon cycle	oceanic and terrestrial carbon cycles (CO_2), tropospheric chemistry and natural wetlands to simulate atmospheric (CH_4, O_3), stratospheric chemistry NO and O_3, 37 halogenated compounds, dynamic surface albedo due to BC deposited on snow and changes in land cover, and aerosols. Anthropogenic emissions incorporate CO_2 from burning fossil fuels and cement production, CH_4, NO, halogenated compounds, CO, NMVCs, SO_2, NH_4, BC, and OC	Impulse Response

The MAGICC emulator is an AOGCM consisting of a hemispherically averaged upwelling diffusion ocean coupled with a globally averaged carbon cycle model and an atmosphere layer [27]. It includes radiative forcings due to CO_2, CH_4, NO, tropospheric aerosols, tropospheric and stratospheric O_3, and various halogenated gases. This emulator, along with the others in this review, has a temporal resolution of 1 year. As with many other climate emulators, the equilibrium climate sensitivity is a primary model parameter [27], [2].

The time-varying ECS is defined using the transient energy balance equation defined for a perturbed climate system. The MAGICC carbon cycle can emulate temperature-feedback effects on the heterotrophic respiration carbon fluxes.

2.4 The AMAP Air Quality and Climate Emulator

AMAP is an Arctic Council Working Group that studies and reports on the status of and threats to the Arctic environment. AMAP provides advice on political actions that would assist Arctic governments in the remediation and prevention of climate change [39].

The AMAP emulator is a climate and air quality emulator that simulates relationships between Earth's air quality, emissions. and climate. The emulator focuses on SLCFs because of their significant impact on Arctic climate and air quality [3], [4], [11], [16]. It includes emissions of CO_2, CH_4, CO, NO_x, volatile organic compounds (VOCs), S, BC, and OC. Since no other climate forcers are considered, warming simulations are probably underestimated by the AMAP emulator [1].

The emulator runs over 4 latitude bands: 60°N to 90°N (Arctic), 28°N to 60°N (Northern Hemispheric midlatitudes (NHML)), 28°S to 28°S (tropics), and 90°S to 28°S (Southern Hemisphere (SH) midlatitudes and Antarctica). The main climate outputs of the emulator are the regional and global temperature perturbation responses [1].

The climate response to pulse emissions of various species is simulated using a highly approximated, linearized mass and energy balance system for Earth. The emulator simulates Earth's average surface air temperature response when forced by a series of instantaneous pulse emissions of different species, which affect the energy balance of the climate system by changing radiative forcings of greenhouse gases and SLCFs. The AMAP emulator simulates the temporal evolution

of the 4 outputted regional mean temperatures using a specified climate sensitivity, time scales of heat dissipation, and Regional Temperature-Change Potentials (RTPs), among other parameters derived from comprehensive ESMs.

Since its first scientific assessment in 1990, the Intergovernmental Panel on Climate Change (IPCC) has employed the Global Warming Potential (GWP) metric to compare the varying climate impacts arising from emissions of different GHGs [40]. The GWP is the radiative forcing due to a pulse emission of a certain species, integrated over a time horizon, relative to a pulse emission of carbon dioxide [40], [41]. This metric can serve as a basis to understanding how the AMAP emulator was developed.

In [41] a linearized energy budget is used to define the Absolute Global Temperature Change Potential (AGTP), in units of [K kg^{-1}], as the global average surface temperature change at a time t after a 1 kg pulse emission at time $t = 0$. This study, in addition to [42] and [43], employed this metric to compare the impacts of different pollutants on Earth's mean surface temperature.

The Absolute Regional Temperature-Change Potential (ARTP) is an extension of the AGTP concept, but on a regional scale as opposed to global, and is employed in the AMAP emulator for simulating regional temperature changes [16], [44], [45]. Additionally, the emulator simulates the heat transport between the 4 geographical regions. As the emulator runs, it generates a temperature response in region m, to a radiative forcing in region l, where $l, m = 1, ..., M$, for the $M = 4$ separate regions, and adds the contributions from each for a net temperature-change effect in region m [1].

The ARTP for a region m is defined as follows, in [K kg^{-1}]:

$$ARTP_m(H) = AGTP(H)g\left(\frac{1}{\lambda\delta F_0}\right)RTP_m, \tag{1}$$

where H is the annual time horizon: the elapsed time between the time of the pulse emission and temperature response. g is a dimensionless scaling parameter. δF_0 represents the global radiative forcing perturbation due to all of the pulse emissions, and λ represents the ECS parameter, in [K/W$\cdot m^2$].

The Regional Temperature-Change Potential (RTP) in region m, in [K], is defined as:

$$RTP_m = \sum_{l=1}^{M} k_{lm} \delta F_{0l} \tag{2}$$

where k_{lm} is a matrix of regional temperature response coefficients [K/W·m^2]. The values in this matrix were derived from simulations with GISS-ER, a coupled atmosphere–ocean climate model [44]. The matrix applies for each of CH_4, CO_2, SO_4, and organic aerosols in the emulator, and are used for different forcing processes, based on the approach used in a previous AMAP BC and O_3 assessment [46]. The λ and δF_0 terms in Equation 1 ensure that the ECS value as shown in Equation 4 matches the global climate sensitivity calculated from integrating the RTPS:

$$ECS_{RTP} = \frac{F_{2x}}{\delta F_0} \sum_m \sum_l k_{lm} \delta F_{0l} z_m \tag{3}$$

$$ECS = \lambda F_{2x} \tag{4}$$

where F_{2x} is the global radiative forcing from doubling of CO2 and z_m is the global area fraction of region m [m^2m^{-2}].

Currently, the ECS parameter λ in the AMAP emulator is scaled by a coefficient g that brings the ECS from 2.7 K to the derived value of 3.7 K from CMIP6, which also matches recent literature [1], [14], [24], [47], [48]. The ECS would be underestimated without this scaling because the coefficient matrix used to define the RTPs, using values from GISS-ER, were found to produce a lower ECS of 2.7 K. GISS-ER has an ECS value that is notably low in the expected range of $2.5 < ECS < 4.0$ K, and has been shown to have a weak response in Arctic sea ice to changes in Arctic temperature [44], [54].

The scaling done in the AMAP emulator that brings the ECS value up to 3.7 K is shown in the equation below:

$$g = \frac{\lambda F_{2x}}{ECS_{RTP}} \tag{5}$$

In the AMAP emulator, the ARTP is used to compute and combine regional temperature responses to series of time-varying pulse emissions, resulting in a series of ARTPs with various time horizons as the number of simulated years increases. These ARTPs are summed to estimate the net regional temperature response in region m to annual mean emissions over N years, beginning with

year t_0 [1]. The total temperature response to emissions of multiple species from the 4 regions are calculated by summing forced temperature changes.

CH_4 is treated by the emulator as a well-mixed GHG without any spatial structure in radiative forcings or dependence on regional emission sources [1]. Its atmospheric lifetime, τ_{CH_4} is modeled as a function of the time scales of other processes:

$$\frac{1}{\tau_{CH_4}} = \frac{1}{\tau_{OH}} + \frac{1}{\tau_{strat}} + \frac{1}{\tau_{soil}} + \frac{1}{\tau_{trop-Cl}} \tag{6}$$

where τ_{OH} is the timescale for CH_4 being destroyed by hydroxyl (OH) radicals, τ_{strat} is the timescale for CH_4 destruction in the stratosphere, τ_{soil} is the time scale for CH_4 uptake by soil, and $\tau_{trop-Cl}$ is the timescale for its reaction with tropospheric chlorine. Each of the contributions are shown in Table 2, resulting in a lifetime of CH_4 of 9.13 years.

Natural emissions of CH_4 are included in the emulator as a constant 202.0 TG/year, using results from [7]. The feedback loop of increased methane concentrations, permafrost thaw, and increased anaerobic respiration from biogenic CH_4 sources is not presently included in the AMAP emulator [11],[13],[49],[50].

Time scale	AMAP Emulator value [yr]
τ_{OH}	11.17
τ_{strat}	120
τ_{soil}	150
$\tau_{trop-Cl}$	200
τ_{CH_4}	9.13

Table 2: Time scales of CH_4 loss processes accounted for in its atmospheric lifetime in the AMAP emulator, following [7], [50], [51], and [52].

As the simulated temperature response of the AMAP emulator is a highly simplified model of Earth's complex processes, the results are most accurate close to the baseline year. The default reference year is 2015, and the default time period of interest is 1990-2050. The simulations beginning in 1990 are based on results from a spin-up emulator simulation from 1850-1990 [1].

2.5 Evaluating the AMAP Emulator and other Emulators

A 2022 study of the AMAP emulator compared projections generated by the AMAP emulator to results from CMIP6, focusing on CO_2 and SLCFs [6]. The emulator output for the Arctic region (60°-90°N) corresponding to specified CO_2 emissions from SSPs was compared to results from CMIP6. These results were found to be comparable to the warming unmasking due to sulfate emission reductions projected by the AMAP emulator. These reductions are often not available in ESMs. This study suggested that the impact of reducing CO_2 emissions could be greatly offset by the unmasking effect from sulfate emission reductions [6].

The AMAP emulator was additionally run for four AMAP-defined comprehensive emissions scenarios were combined for air pollutants and GHGs to evaluate the effects of emission reductions on climate and human health. It was found that technically feasible emissions reduction scenarios could result in simultaneous climate and human health benefits [6].

In 2022, [8] performed an evaluation of 18 state-of-the-art models and their performance for simulating SLCFs. These models included ESMs, RCMs, CTMs (Chemical Transport Models), Chemistry-Climate Models (CCMs), and GCMs (General Circulation Models). The ways these models represent SLCFs in the Arctic and Northern Hemisphere were evaluated by comparing the results of simulations over 4-year periods (2008–2009 and 2014–2015) from these models to observational data. Though not each model included the same set of species, BC, CH_4, sulfate, tropospheric O_3 and its precursors, organic aerosols, and particulate matter were included when possible for each model.

Absolute and relative model biases were used as the primary metric for evaluating the model output, including annual means, seasonal cycles, and 3-D distributions. The multi-model mean was able to represent the general features of SLCFs in the Arctic and had the best overall performance. For CH_4, O_3, BC, and sulfate, which have great radiative impacts, the multi-model mean was within $\pm 25\%$ of the measurements across the Northern Hemisphere. This demonstrated that using a multi-model ensemble to simulate the climate and health impacts of SLCFs would be optimal.

2.6 Synthesis

SLCFs are highly impactful on human health and climate change, especially in the Arctic [3], [4]. Comprehensive ESMs are used to simulate projected warming and air quality, but are computationally expensive, so less resource-intensive alternatives for climate and air quality are highly useful, especially in policy-making settings [2], [3], [1]. The effects of SLCFs on climate and their associated feedbacks (ie, cloud-related feedbacks) require a more focused study, as some of these radiative impacts and feedbacks remain a high source of uncertainty in climate modelling [14], [53]. The AMAP emulator is a new tool that can be used to simulate projected air quality and climate for various emissions scenarios, but it has limitations, such as its underestimation of Arctic amplification, and very simple model of atmospheric CH_4 [1], [6]. Improvements to the emulator on these aspects are the focus of this study.

Arctic warming rates have been shown to be projected lower by the AMAP emulator than by cutting edge ESMs included in CMIP6. This is due to the RTP coefficients used by the emulator originating from simulations from an ESM (GISS-ER) with a relatively low ECS value of 2.7 K and weak Arctic warming responses [1], [6], [14], [24], [47], [48], [54]. The coefficients for the Arctic RTP, RTP_{ARC}, could benefit from modification.

Regenerating these coefficients with a different or modified comprehensive ESM would be highly resource-intensive, but the AMAP emulator can be used to diagnose how underestimated the Arctic RTP coefficients.

The positive feedback loop of increased CH_4 concentrations, permafrost thaw, and increased anaerobic respiration from biogenic CH_4 sources is not presently included in the AMAP emulator [11], [13], [49], [50]. Natural emissions of CH_4 are instead modelled as a constant 202.0 Tg/year.

The three main objectives of this study include diagnosing the differences between the AMAP emulator and the most cutting edge ESMs, the modification of the AMAP emulator's RTP coefficients k_{lm} to better emulate Arctic temperatures, and adapting CH_4's representation in the emulator to include a positive feedback loop of natural CH_4 emissions and increases in Arctic temperature.

3 Methods

3.1 Evaluating the AMAP Emulator

3.1.1 Extending and Existing Study

A comparison of AMAP emulator projections of Arctic and global temperature against CMIP6 results for various emissions scenarios was conducted to verify and further diagnose inconsistencies between the AMAP emulator and recent, cutting-edge comprehensive ESMs involved in CMIP6. This comparison approach was identical to the approach taken for the comparison between AMAP emulator and CMIP6 results conducted in [6], but the points of comparison were different, and an extra scenario (SSP1-1.9) was added. Table 6 in Appendix A lists the CMIP6 ESMs that were included in the ensemble for each SSP in this comparison. These ESMs have ECS values of $2.5 < ECS < 4.0$ K, which is an expected range of the true ECS value based on the results from the IPCC Sixth Assessment Report and other recent studies [6], [12], [53].

This comparison included five scenarios, including SSP1-1.9, SSP1-2.6, SSP2-4.5, SSP3-7.0, and SSP5-8.5. The SSP nomenclature begins with the umbrella scenario followed by the expected radiative forcing in 2100, in [W m^{-2}], so SSP5-8.5, a fossil-fuel development scenario, is the scenario most impacted by global warming, with an expected radiative forcing of 8.5 W m^{-2} in 2100 [26].

A range of realizations with different radiative forcing due to aerosols was constructed to estimate the uncertainties of the projections. For each SSP, the AMAP projections were averaged over projections with two perturbation values (a high and a low value) for aerosol/cloud interactions, aerosol/radiation interactions, and aerosol/snow interactions. These values were the same as used in [6].

The resulting mean surface air temperature difference from the five SSPs were normalized to be relative to 1995-2014 as opposed to their original reference to the year of 1750. The reference period of 1995-2014 is exclusively in this study. This is the reference time period of the ESM simulations in CMIP6, which allowed for direct comparisons between CMIP6 results and AMAP emulator projections through realizing SSPs. This was completed for the aerosols, CO_2, and CH_4 components of the emulator. Though O_3 can be simulated by the emulator, O_3 projections were

not included due to an unavailability of emissions information. Warming due to O_3 projected by the AMAP emulator has been shown to be relatively low compared to other species [6].

For each of the five SSPs, a set of realizations from CMIP6 ESMs was averaged. The normalized AMAP emulator projections until were compared to the results results from CMIP6 for 2030 and 2050.

3.1.2 Comparing the AMAP Emulator Results with a Larger CMIP6 Ensemble

To further evaluate the AMAP emulator, its output was also compared against the output of a second CMIP6 ensemble, which included a larger spread of ESMs. This ensemble will be referred to as the large CMIP6 ensemble. For comparison with the AMAP emulator output, 27 CMIP6 realizations of four SSPs (SSP1-2.6, SSP2-4.5, SSP3-7.0, and SSP5-8.5) were processed to construct time series of the global and regional surface air temperatures. These 27 realizations included one realization from each of the following ESMs: AWI-CM-1-1-MR, BCC-CSM2-MR, CAMS-CSM1-0, CanESM5, CESM2-WACCM, CESM2, CMCC-CM2-SR5, CNRM-CM6-1, CNRM-ESM2-1, EC-Earth3-Veg, EC-Earth3, FGOALS-f3-L, FGOALS-g3, GFDL-ESM4, IITM-ESM, INM-CM4-8, INM-CM5-0, IPSL-CM6A-LR, KACE-1-0-G, MIROC-ES2L, MIROC6, MPI-ESM1-2-HR, MPI-ESM1-2-LR, MRI-ESM2-0, NorESM2-LM, NorESM2-MM, UKESM1-0-LL.

A larger ensemble of CMIP6 results including realizations from a mix of ESMs from CMIP6 for SSP1-1.9, SSP1-2.6, SSP3-7.0, and SSP5-8.5, but due to reduce biases across comparisons of SSPs, ESMs that did not provide a realization for each of the SSPs were excluded, and SSP1-1.9 was not included.

The same set of realizations generated by the AMAP emulator for the previous section were averaged for each SSP for comparison against this CMIP6 ensemble, with 2 additional realizations: realizations with an ECS value scaled to 2.59 K and 5.00 K. This yielded a total of 24 realizations for each SSP.

The following workflow was used to process and analyze the AMAP emulator output for each of the SSPs.

Mean Global Regional Surface Air Temperatures

The 24 realizations of the AMAP emulator were averaged to create a time series of the average surface air temperature for each region. The uncertainties of the regional average surface air tem-

peratures each year were taken as the standard deviation of the temperatures in the ensemble for that year.

Global and Regional Surface Air Temperature Anomalies

The evolving temperature anomalies for each region, relative to a reference period of 1995-2014, were found by subtracting the reference period temperature from the time series. A global time series of surface air temperature anomalies was also created by summing the temperature anomaly contributions from each region for each year.

Regional Amplifications

Finally, a time series of regional temperature amplifications was constructed. The regional temperature amplification for a given year was modelled as the ratio of the regional temperature anomaly, relative to the 1995-2014 reference period, to the global temperature anomaly.

Regional amplification was additionally studied as a function of global surface air temperature anomaly versus the regional surface air temperature anomaly. The time series of the global and regional amplifications were linearly fit using reduced major axis regression, which estimated slopes μ_{gm}, where g represents the global SAT anomaly as the independent variable, and m represents the index region of interest. Reduced major axis regression was used because there was a high level of uncertainty in both the global and regional temperature anomalies, and this type of regression produces the same results regardless of which variable is the ”dependent” or ”independent” variable [55], [56].

This same workflow was completed for the 27-member ensemble of CMIP6 realizations for each of the SSPs, for comparison with the AMAP emulator results. The mean relative difference in projected mean surface air temperature change, Δ_{rel}, the coefficient of variation, a regional amplifications represented as regional surface air temperature anomalies relative to global surface air temperature anomalies were also used as metrics for quantifying how well the AMAP emulator output captured the CMIP6 results over time.

3.2 Tweaking RTP Coefficients

In order to tweak Arctic amplification projected by the AMAP emulator to better match the most recent comprehensive ESMs, 15 of the 16 RTP coefficients k_{lm} were modified. Since these coeffi-

cients have been shown to result in underestimated Arctic warming and an overall underestimated ECS, an increase to the Arctic RTP coefficients would necessarily result in increased Arctic warming.

The existing RTP coefficients used by the AMAP emulator were incrementally increased to test how resulting temperature projections would correspond to the CMIP6 results.

The coefficients were scaled up by a coefficient δ with an area-weighted decrease in the coefficients for the other regions. The resulting ECS value from the RTPs was thus kept constant, as a control variable equal to 2.7 K before scaling to 3.7 K.

The 4×4 matrix of RTP coefficients was modified and studied for four cases. The area-weighted sum of the Arctic RTP coefficients were increased by a fraction δ, while the RTP coefficients for the other regions were correspondingly decreased with an area-based weighting. This was done to result in a system with the same ECS value as the default AMAP emulator settings. The resulting modified RTP coefficients for each of the δ values that were tested are shown in Table 7 in Appendix B. The only coefficient that was unchanged by this method was the RTP coefficient corresponding to the contribution of warming in the Southern Hemisphere corresponding to changes in the Arctic, $k_{ARC,SH}$, because this coefficient was equal to zero in the default settings.

The first case, or base case, involved a δ value of zero, and corresponded to the existing default settings of the emulator. The case with $\delta = 0.5$ was conducted to estimate a ceiling for a maximal adjustment of the RTP_{ARC} value. This study included tests with $\delta = \{0.00, 0.10, 0.25, 0.50\}$.

For each of the δ values, the AMAP emulator was run for projections of aerosols, CH_4, and CO_2, but not O_3.. The k_{lm} coefficients were changed for effects from organic and sulfate aerosols, CH_4, and CO_2, sulfate aerosols.

For each setting of δ, the AMAP emulator was run to create an ensemble of 24 members for SSP5-8.5, with the same ensemble members as specified in 3.1.2.

3.2.1 Processing the Emulator Results and CMIP6 Results

The same workflow as described in section 3.1.2 was completed to analyze the AMAP emulator output for each of the δ settings. These results were compared against the large 27-member ensemble of CMIP6 realizations for SSP5-8.5.

3.3 Incorporating a Feedback Loop for Methane Emissions

A simple feedback loop linking CH_4 emissions and Arctic temperature, to emulate the feedback occurring due to permafrost thaw, was added to the AMAP emulator and evaluated. The loop is shown in Equation 7, where $E_{CH_4}(t)'$ is the natural emission of CH_4 in year t, in Tg, E_{CH_4}=202.0 Tg, α is a specified dimensionless weight, and $dT_{ARC}(t-1)$ is the mean Arctic temperature projected by the AMAP emulator in the prior year.

$$E_{CH_4}(t)' = E_{CH_4}\left(1 + \alpha \cdot ReLU(dT_{ARC}(t-1))\right), \tag{7}$$

$$ReLU(T) = \begin{cases} 0, & T \leq 0 \\ T, & T > 0 \end{cases}$$

An implementation of this feedback loop with α values of 0.00 (default), 0.10, 0.25, and 1.00 was tested for SSP5-8.5 to test the impact on a high radiative forcing scenario.

4 Results and Discussion

4.1 Evaluating the AMAP Emulator

As the AMAP emulator is a highly simplified model of Earth's climate system components, it is valuable to first observe how its output compares to the output of more comprehensive ESMs over time.

Figure 1 presents a time series of the mean global and regional surface air temperature anomalies projected by the AMAP emulator, for the large ensemble. The projected anomalies diverge over time for different SSPs projected by AMAP emulator as expected, with SSP5-8.5, a "fossil fuel development" pathway in which the global radiative forcing in 2100 is 8.5 W m^{-2}, consistently resulted in the greatest projected warming across all regions. Likewise, SSP1-2.6, a "sustainable" pathway in which the global radiative forcing in 2100 is only 2.6 W m^{-2}, consistently resulted in the greatest projected warming across all regions.

This figure shows that in general, differences in projected SAT anomaly across the SSPs, on a global regional scale, generally become most apparent beyond the year 2030. The greatest regional

anomalies were found to occur in the Arctic, with the greatest anomaly occurring in 2050 for SSP5-8.5, the pathway with the greatest future radiative forcing. In 2050, the AMAP emulator projects an Arctic anomaly of 4.54 ± 0.47 °C and an overall global anomaly of 2.79 ± 0.29 °C.

In contrast to this, time series depicting the large CMIP6 ensemble is shown to yield much greater uncertainties, due to the individual biases of the 27 ESMs included and their internal variability. This is shown in Figure 2. Here, the greatest regional anomaly projected by this ensemble is the Arctic anomaly for SSP5-8.5, an estimated anomaly of 3.46 ± 2.15 °C. The overall global anomaly for 2050 in SSP5-8.5 is projected to be 1.61 ± 0.69 °C.

The higher variance of results in the CMIP6 ensemble compared to the variance seen in the set of AMAP realizations is further illustrated in Figures 14 and 15, wherein the regional amplifications of individual realizations are shown for the year 2050, for four SSPs.

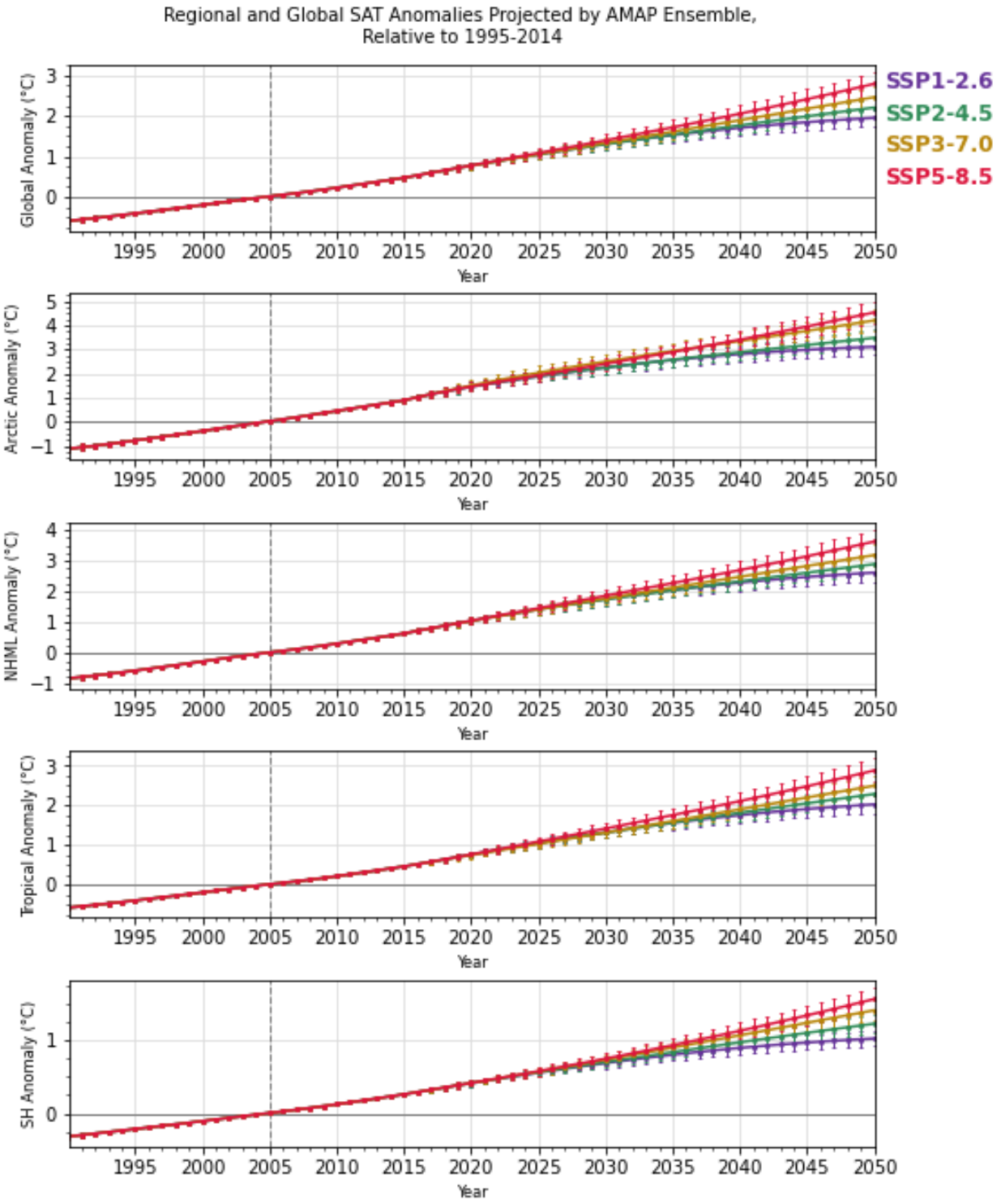

Figure 1: Time series of the regional and global surface air temperature anomalies projected by the AMAP emulator, for four SSPs, relative to a reference period of 1995-2014. The standard deviation of the temperatures realized for each year was taken as the SAT anomaly uncertainty for that year.

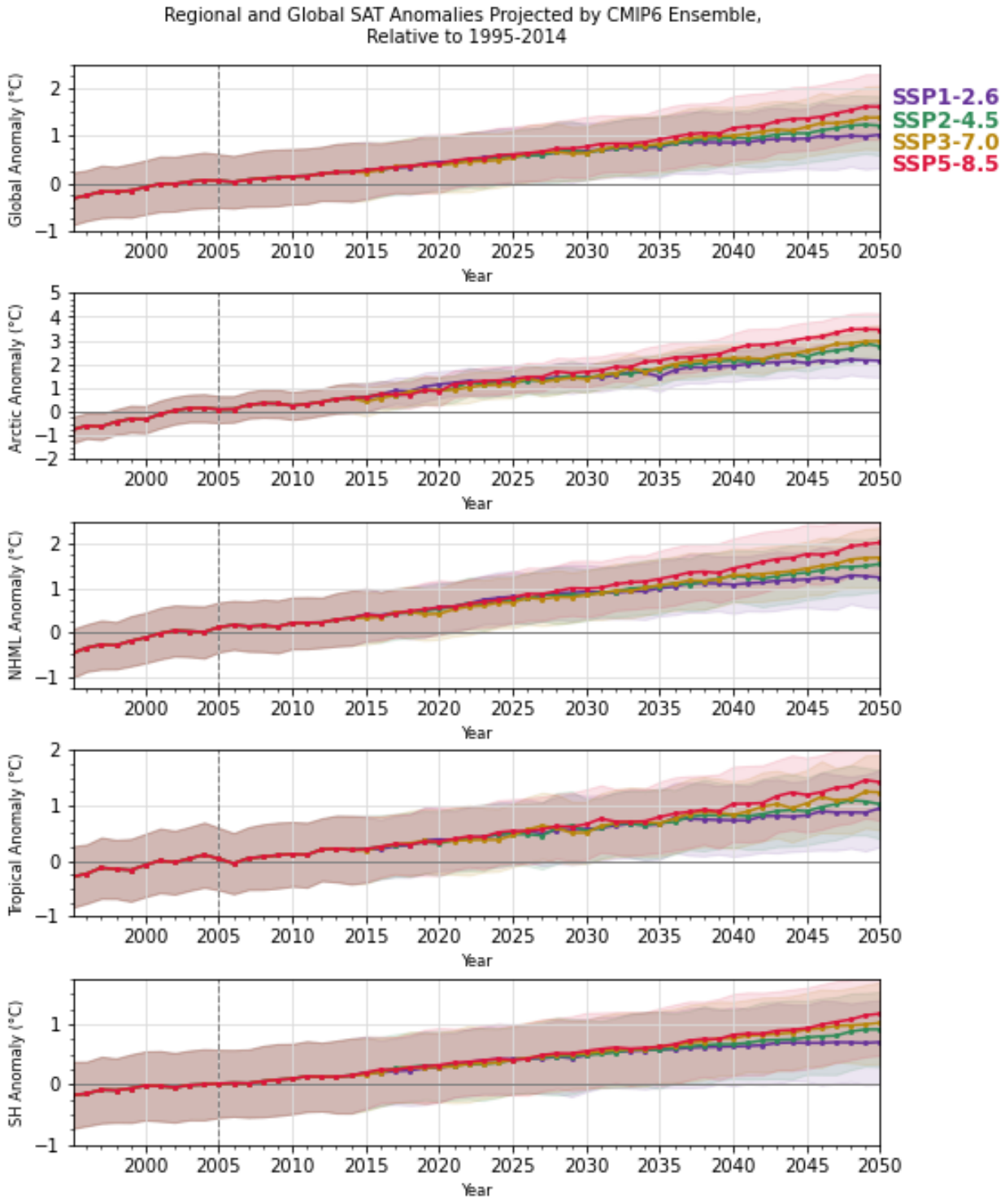

Figure 2: Time series of the regional and global surface air temperature anomalies projected by the AMAP emulator, for four SSPs, relative to a reference period of 1995-2014. The standard deviation of the temperatures realized for each year was taken as the SAT anomaly uncertainty for that year.

Returning to the smaller, augmented ensembles as from [6], the results for the comparison of the AMAP emulator and CMIP6 ensemble results for 2050 are shown in Figure 3, and the comparison for 2030 is shown in Figure 4.

Table 3 shows corresponding the mean relative difference of the results across the five SSPs for each region/year combination. The mean relative difference Δ_{rel} is defined in Equation 8, where there are $N = 5$ SSP scenarios, and x_i and y_i represent the estimated temperature difference from the AMAP emulator and CMIP6 results, respectively. The mean absolute difference, Δ_{aba}, is defined in Equation 9.

$$\Delta_{rel} = \frac{1}{N} \sum_{i=1}^{N} \frac{x_i - y_i}{(x_i + y_i)/2} \cdot 100\% \tag{8}$$

$$\Delta_{abs} = \frac{1}{N} \sum_{i=1}^{N} (x_i - y_i) \tag{9}$$

As made apparent by Figure 3, in 2050, there is an overall trend of global warming being overestimated and Arctic warming being underestimated by the AMAP emulator, corresponding to mean relative differences of $19.3 \pm 16.0\%$ and $-22.4 \pm 27.0\%$, respectively. This is in accordance with the findings from [6], and is indicative of underestimated Arctic amplification.

The AMAP emulator's underestimation of Arctic warming is less evident in Figure 4, which shows projection results until 2030, which shows a much smaller but still negative mean relative difference of $-5.0 \pm 31.5\%$. The uncertainties of these comparisons are extremely high to to the propagated uncertainties from the CMIP6 and AMAP projecting highly uncertain processes, as well as internal variability [14] [57].

Year	Region	Δ_{rel}	Δ_{abs} []
2030	Arctic	-5.0 ± 31.5	0.2 $\pm 0.5\%$
2030	Global	20.5 ± 15.7	0.1 $\pm 0.1\%$
2050	Arctic	-22.4 ± 27.0	0.5 $\pm 0.6\%$
2050	Global	19.3 ± 16.0	0.2 $\pm 0.2\%$

Table 3: Mean relative and absolute differences corresponding to Figures 4 and 3, across the five SSPs.

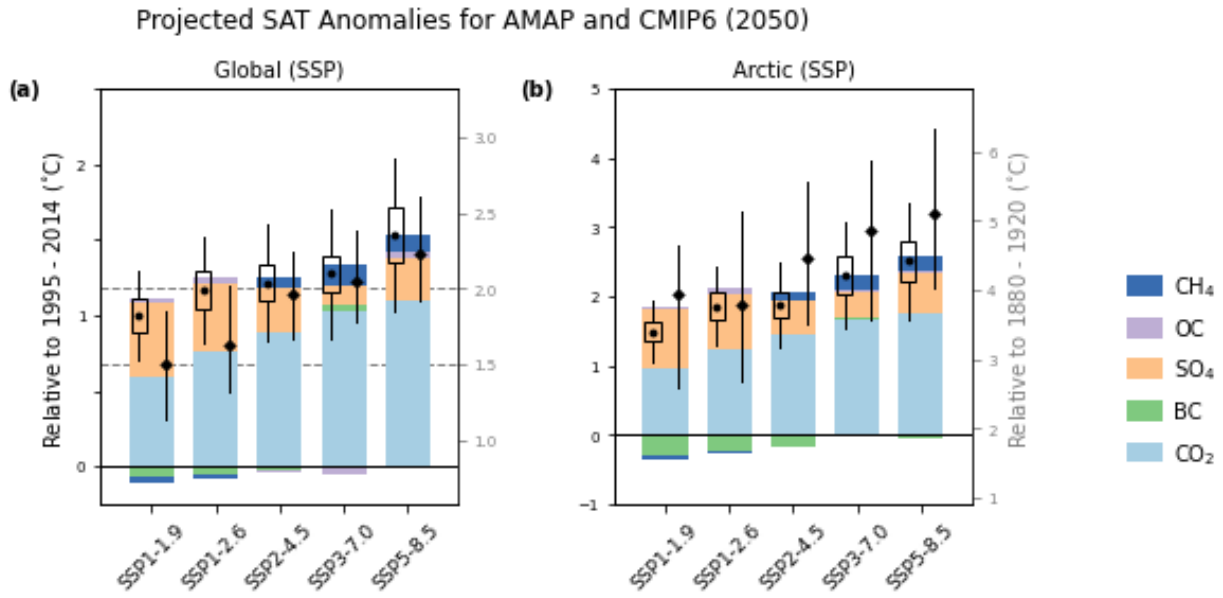

Figure 3: Projected global and Arctic mean surface air temperature changes in 2050. The net temperature changes projected by the AMAP emulator are plotted as circles, the CMIP6 multi-model median values as diamonds. The 5–95% confidence intervals ($\pm 1.64\sigma$), resulting from uncertainties in all simulated processes, are shown as black error bars. Confidence ranges due to radiative forcing uncertainty in the AMAP emulator are shown as rectangles. Color bars refer to the forced temperature change from the individual air pollutant and greenhouse gas species, based on AMAP emulator simulations. Warming relative to preindustrial conditions is also indicated (grey font, with 1.5 and 2 °C thresholds indicated by dashed lines in (a)).

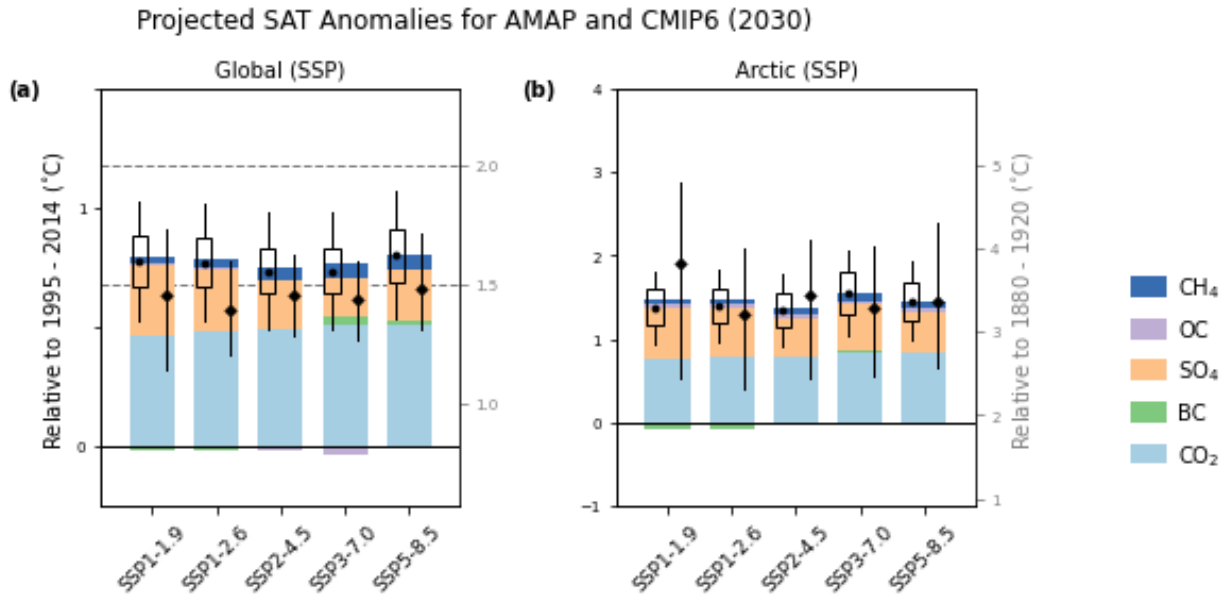

Figure 4: Same as Figure 3, but for the year 2030.

A notable outlier from the 2030 comparison, in Figure 4(b), is that the mean absolute difference in the projected Arctic surface air temperature anomaly between the AMAP emulator and CMIP6 results is significantly greater in magnitude for SSP1-1.9 than for the other scenarios (0.5 ± 1.4°C for SSP1-1.9 vs an average of 0.1 ± 0.5°C across the other four SSPs). This may be largely due to the much smaller pool of CMIP6 data included in the comparison for this SSP. For this comparison, realizations from only five ESMs were included, while comparisons with the other four SSPs included realizations from 13 or more ESMs (see Table 6 in Appendix A).

As is seen on the results from Figures 3 and 4, the species generally contributing to the greatest SAT anomaly is CO_2, followed by sulfate aerosols and CH_4. Reductions in sulfate emissions unmasks some Arctic warming in each of the scenarios, intensifying the radiative impacts of other species.

Figures 5 and 6 show a time series of the regional amplifications for each of the four regions simulated by the AMAP emulator.

In Figure 5, the regional amplifications projected by the AMAP emulator generally coincide smoothly over time, with some exceptions. SSP3-7.0 shows notably and consistently higher Arctic amplification and lower tropical amplification. The difference in Arctic amplification may be attributed to the significantly higher CH_4 emissions for that SSP, which exacerbates Arctic warm-

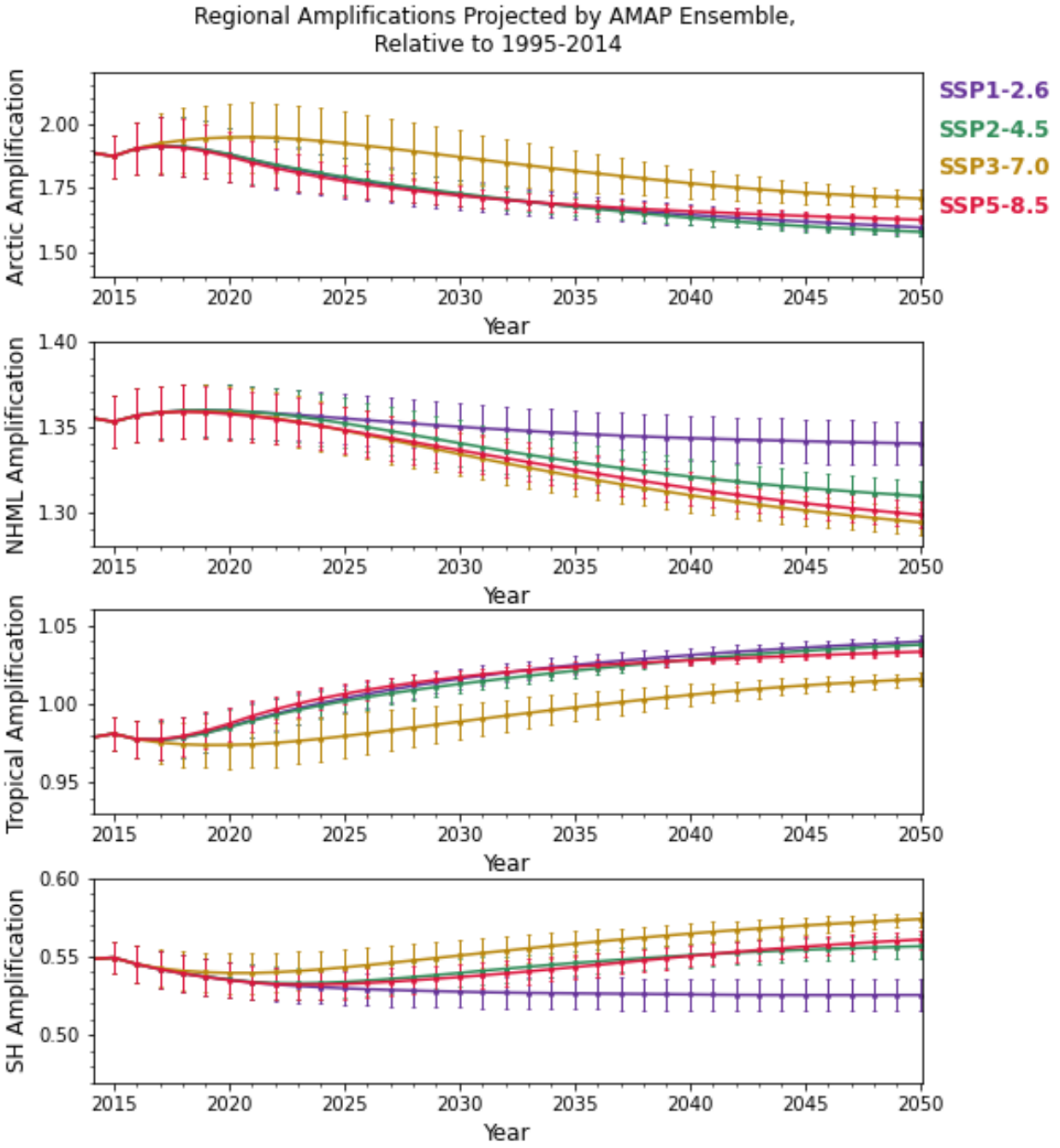

Figure 5: Time series of the regional amplifications for the 4 regions projected by the AMAP emulator, for SSP1-2.6, SSP2-4.5, SSP3-7.0, and SSP5-8.5. The regional amplification for each year is represented as the ratio of the average regional SAT anomaly across the ensemble (with reference to the period of 1995-2014) to the average global SAT anomaly. The error bars represent the propagated uncertainty of the two mean SAT anomalies in the dividend (regional and global).

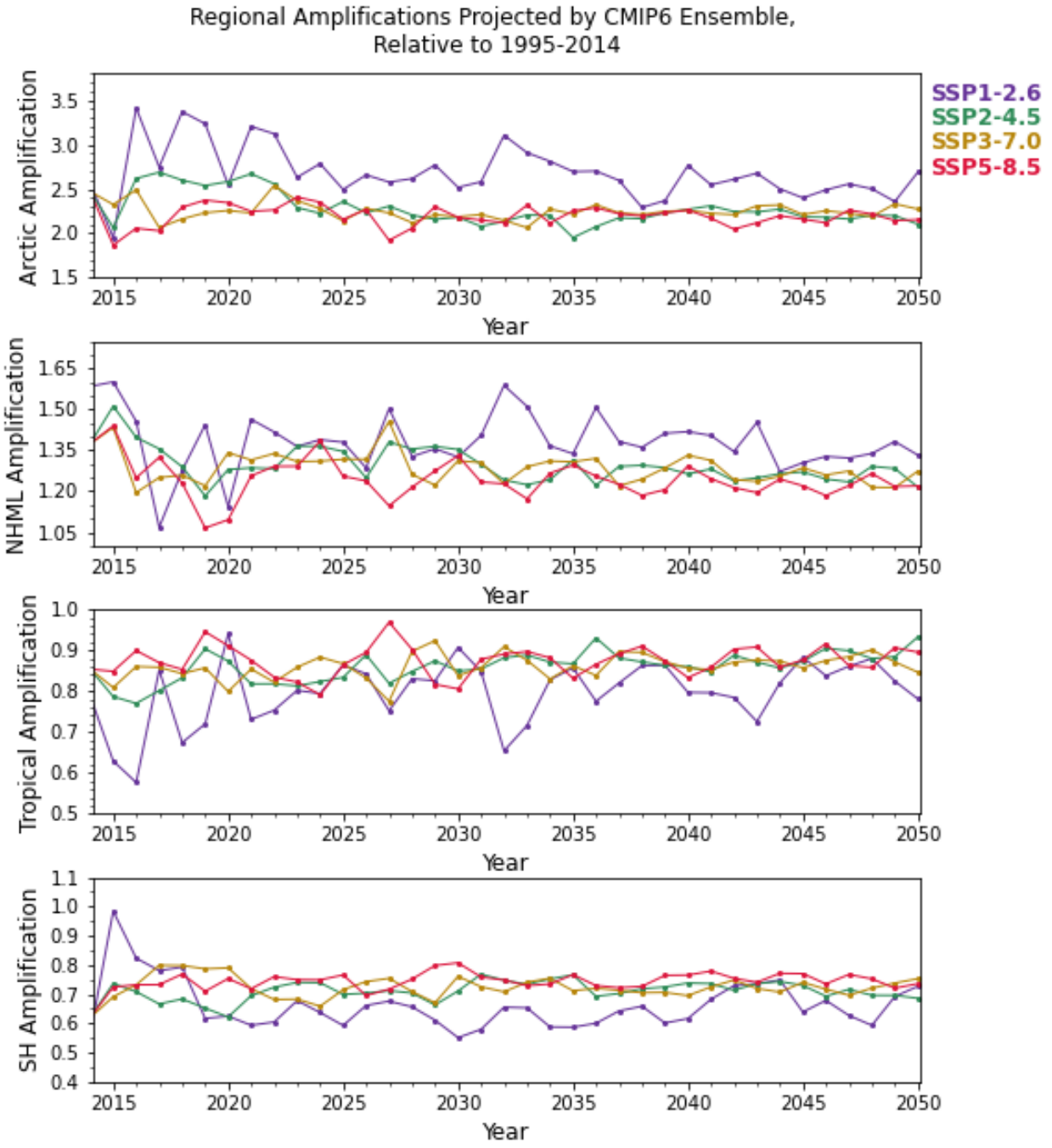

Figure 6: Same as Figure 5, but for the CMIP6 ensemble. Error bars are neglected in this figure to focus on the variation across the SSPs. A version of this plot with error bars is shown in Appendix C, Figure 13.

ing [58]. Another notable difference across the SSPs in these time series is that for SSP1-2.6, regional amplification in the Northern Hemisphere midlatitudes and in the Southern Hemisphere are consistently higher and lower respectively than the general trend shown by the other SSPs.

For the CMIP6 projections of the Arctic warming, the regional amplification time series for the four SSPs have greater variances over time than for the other regional amplification time series. The Arctic amplification for SSP1-2.6 deviates considerably more over time compared to the other SSPs; this is likely because the ESMs included in the CMIP6 ensemble do not have as unified a equilibrium climate sensitivity, and this is especially apparent through weaker radiative forcing than stronger forcing.

For 2050, the CMIP6 ensemble projects an Arctic amplification of 2.16 ± 0.34 ° C / ° C, while the AMAP emulator ensemble projects an Arctic amplification of 1.63 ± 0.15 °C / ° C. In general, over time, Arctic amplification is generally underestimated by the emulator, relative to the CMIP6 ensemble. This does not necessarily mean that the Arctic warming is underestimated, as is shown in the Arctic temperature anomalies projected by the CMIP6 and AMAP ensembles in 2050.

Additionally, the same regional surface temperature anomalies predicted by the AMAP emulator for each of the SSPs were taken as a function of the global anomalies. The resulting slopes and resulting plots for the AMAP and CMIP6 ensembles are shown in Figures 8 and 7, respectively. For each of the regions, the mean of the estimated slopes across the four SSPs was computed for both the AMAP emulator and CMIP6 ensemble, and is shown in Table 4. The uncertainties of these estimated slopes are notably low, as the uncertainties of the points were not accounted for in the reduced major axis (RMA) regression. Therefore, the uncertainties of these slopes are certainly underestimated, but they still reveal underlying trends between the AMAP emulator and CMIP6 ensemble of ESMs.

From Table 4, it can be gleaned that the AMAP emulator greatly underestimates warming amplification in the Southern Hemisphere as well as in the Arctic.

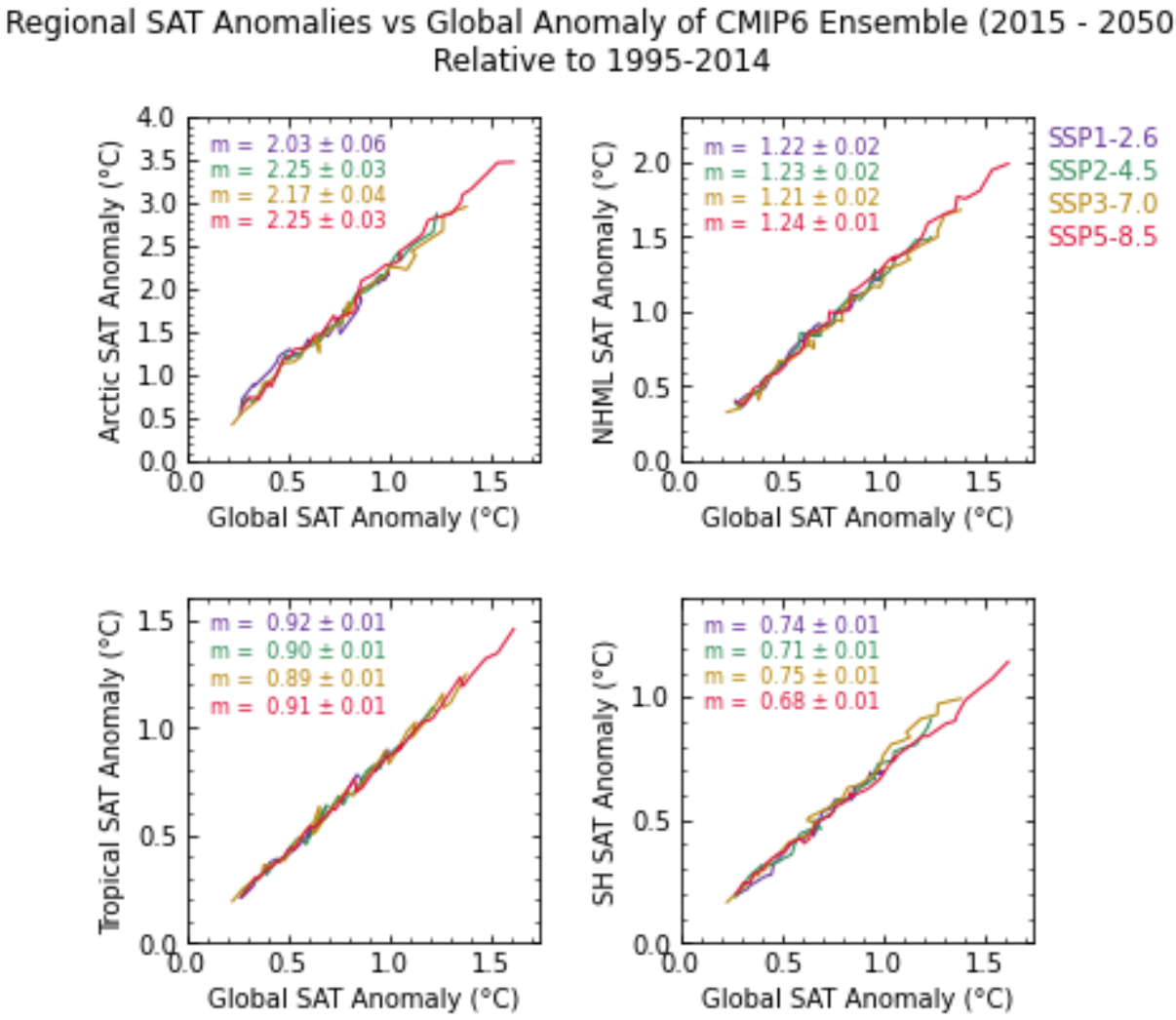

Figure 7: Results of RMA fitting of global versus regional SAT anomalies from the large CMIP6 ensemble for four SSPs, along with the resulting slopes m from the fits

	$\bar{m}_{Arctic}$	$\bar{m}_{NHML}$	$\bar{m}_{Tropical}$	$\bar{m}_{SH}$
AMAP Emulator Ensemble	1.63±0.01	1.31±0.01	1.03±0.01	0.55±0.01
CMIP6 Ensemble	2.18±0.02	1.22±0.01	0.90±0.01	0.72±0.01

Table 4: Mean of estimated slopes of global versus regional surface temperature anomalies [°C / °C], across SSP1-2.6, SSP2-4.5, SSP3-7.0, and SSP5-8.5. The uncertainty of these average slopes were taken by propagating the uncertainties of the individual slopes.

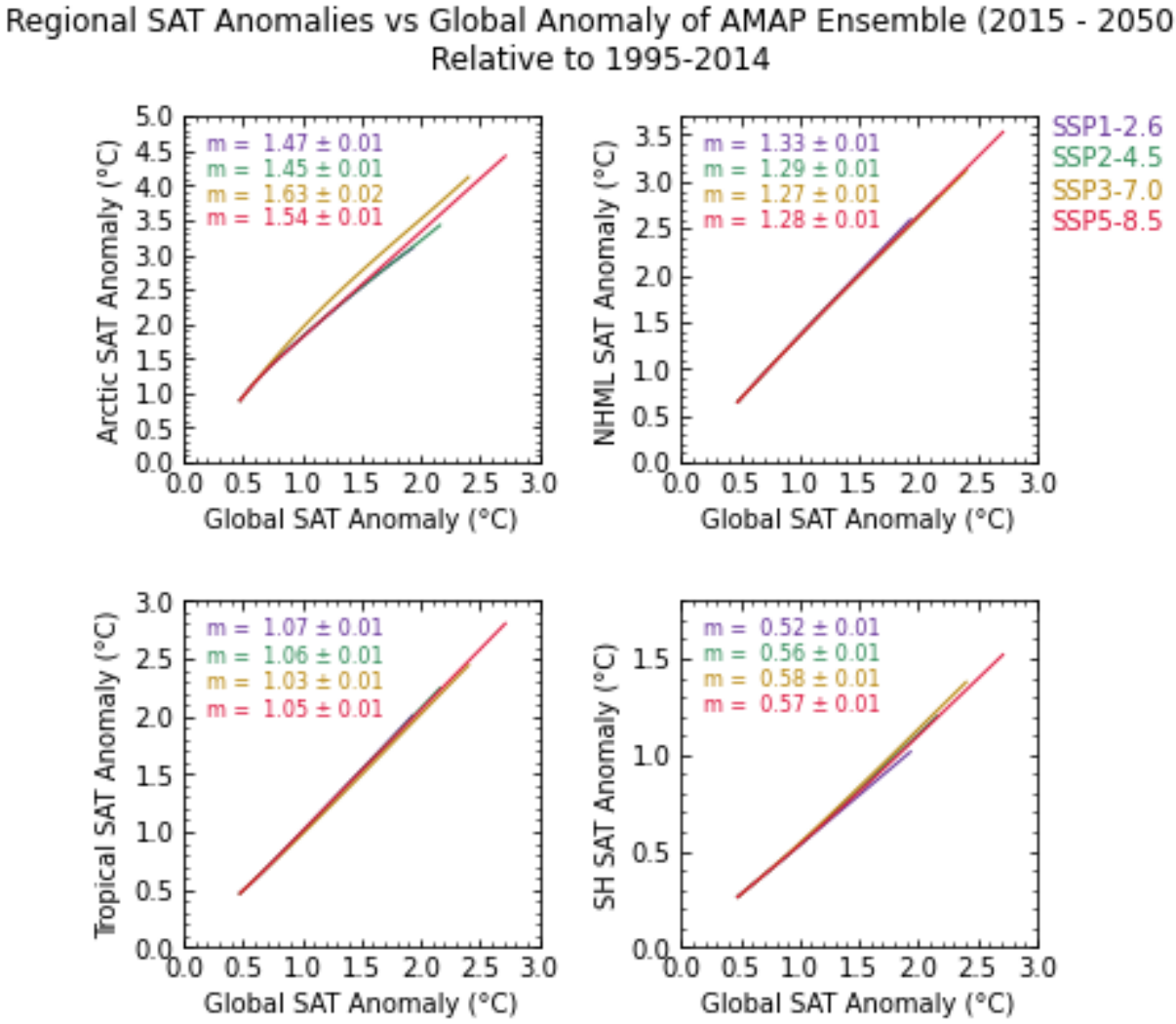

Figure 8: Results of RMA fitting of global versus regional SAT anomalies from AMAP ensemble for four SSPs, along with the resulting slopes m from the fits.

4.2 Tweaking RTP Coefficients

The resulting time series of the AMAP emulators projections for tweakings of $\delta = \{0.00, 0.10, 0.25, 0.50\}$ for SSP5-8.5 are shown in Figure 9. The small differences in global temperature anomalies in the settings where $]delta > 0$ can be attributed to the roundoff error of the modified RTP coefficients. For a given region, the projected anomalies for each of the AMAP emulator settings spread apart over time as the modified weighting of the RTP coefficients becomes increasingly apparent. The time series of surface temperature anomalies projected for different settings are shifted upwards with increasing values of δ, while the anomalies correspondingly decrease in the other regions.

Due to the unchanged ECS value, the global surface air temperature anomalies remain overestimated compared to the CMIP6 SSP5-8.5 results while the regional surface temperature anomalies projected by the AMAP emulator shift in magnitude as the δ value is changed.

Changes in regional amplification projected by the AMAP emulator over increasing values of δ are shown in Figures 5. In general, the CMIP6 ensemble average Arctic amplification is projected to sit between the results from the AMAP emulator for $\delta = 0.25$ and $\delta = 0.50$. The uncertainty in the CMIP6 ensemble results are, however, quite high, as demonstrated in Figure 13 in Appendix C.

The tropical amplification underestimated by the AMAP emulator is carried closer to the CMIP6 results with increasing δ values as tropical warming is decreased and global anomalies stay approximately the same. The regional amplification predicted for the Southern Hemisphere becomes increasingly underestimated with increasing δ.

The regional surface temperature anomalies predicted by the tweaked AMAP emulator for SSP5-8.5, for each of the tested values of δ were taken as a function of the global anomalies to better illustrate the overall correlation across the time series. The resulting slopes and resulting plots for the tweaked AMAP emulator and CMIP6 ensembles are shown in Figure 11 and summarized in Table 5. As previously discussed, the uncertainties of these slopes are greatly underestimated.

As the RMA-fitted slope for the CMIP6 ensemble lies between the RMA-fitted slopes for the AMAP emulator for δ values of .25 and 0.50, an increase in RTP_{ARC} between 25% and 50% could be appropriate to better represent Arctic amplification. Notably, the ECS value was kept constant for this study, but it does have the potential to be changed. Additionally, while the regional

amplification is improved, by increasing the Arctic RTP coefficients, the already overestimated Arctic warming is further increased.

	$\bar{m}_{Arctic}$	$\bar{m}_{NHML}$	$\bar{m}_{Tropical}$	$\bar{m}_{SH}$
AMAP Emulator Ensemble	1.66±0.01	1.31±0.01	1.03±0.01	0.55±0.01
Modified AMAP Emulator Ensemble, $\delta = 0.10$	1.80±0.01	1.29±0.01	1.02±0.01	0.55±0.01
Modified AMAP Emulator Ensemble, $\delta = 0.25$	2.02±0.01	1.26±0.01	1.01±0.01	0.54±0.01
Modified AMAP Emulator Ensemble, $\delta = 0.50$	2.40±0.02	1.21±0.01	0.99±0.01	0.52±0.01
CMIP6 Ensemble	2.25±0.03	1.24±0.01	0.91±0.01	0.68±0.01

Table 5: Mean resulting slopes of global versus regional SAT anomalies [°C / °C] for SSP5-8.5. The uncertainty of these average slopes were taken by propagating the uncertainties of the individual slopes.

4.3 Incorporating a Feedback Loop for Methane Emissions

The results of testing the linear feedback loop proposed in Equation 7 is shown in Figure 12. Preliminary sensitivity test results are shown in Figure 12. Beyond a certain limit, it is expected that the positive feedback loop proposed would dominate in a manner that is unrealistic. Figure 12 demonstrates than an $\alpha = 1.00$ setting is much to high to reasonably reflect the CH_4 feedback loop being modeled [11], [7].

5 Conclusion

SLCFs can have a great impact on human health and climate change, particularly in the Arctic [3], [4]. The AMAP climate emulator is a new emulator that can be used to rapidly generate projections of global surface temperature for four latitude bands. As a highly simplified mass and energy balance model representing Earth's complex chemical and physical processes, the emulator has limitations, such as its underestimation of Arctic amplification, and very simple model of atmospheric CH_4 [1], [6].

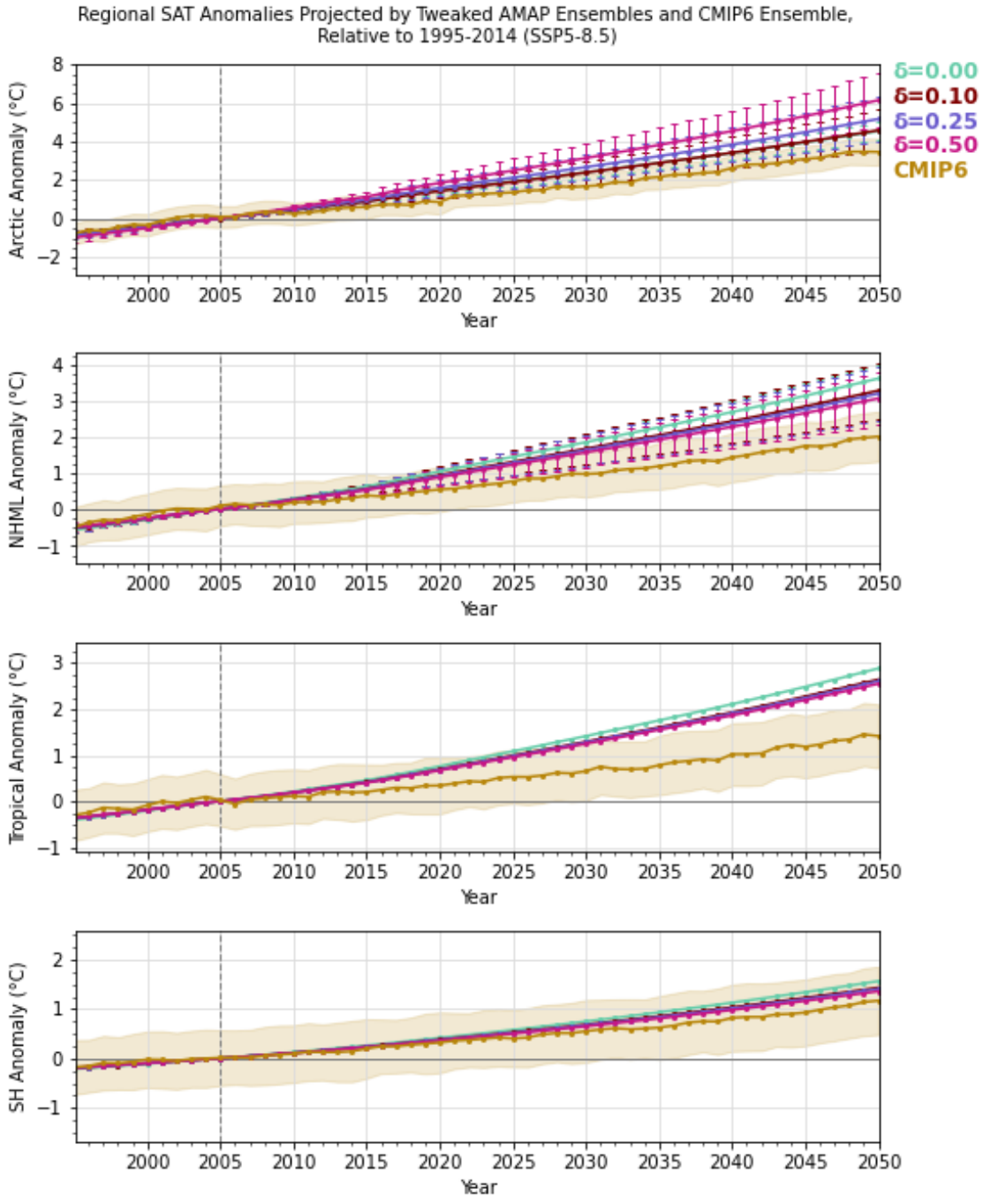

Figure 9: Time series of the regional surface air temperature anomalies projected by the AMAP emulator with tweaked RTP coefficients (different δ settings), relative to a reference period of 1995-2014. The standard deviation of the temperatures realized for each year was taken as the SAT anomaly uncertainty for that year. These results are shown for SSP5-8.5, and are plotted alongside the projected surface air temperature anomalies from the CMIP6 ensemble.

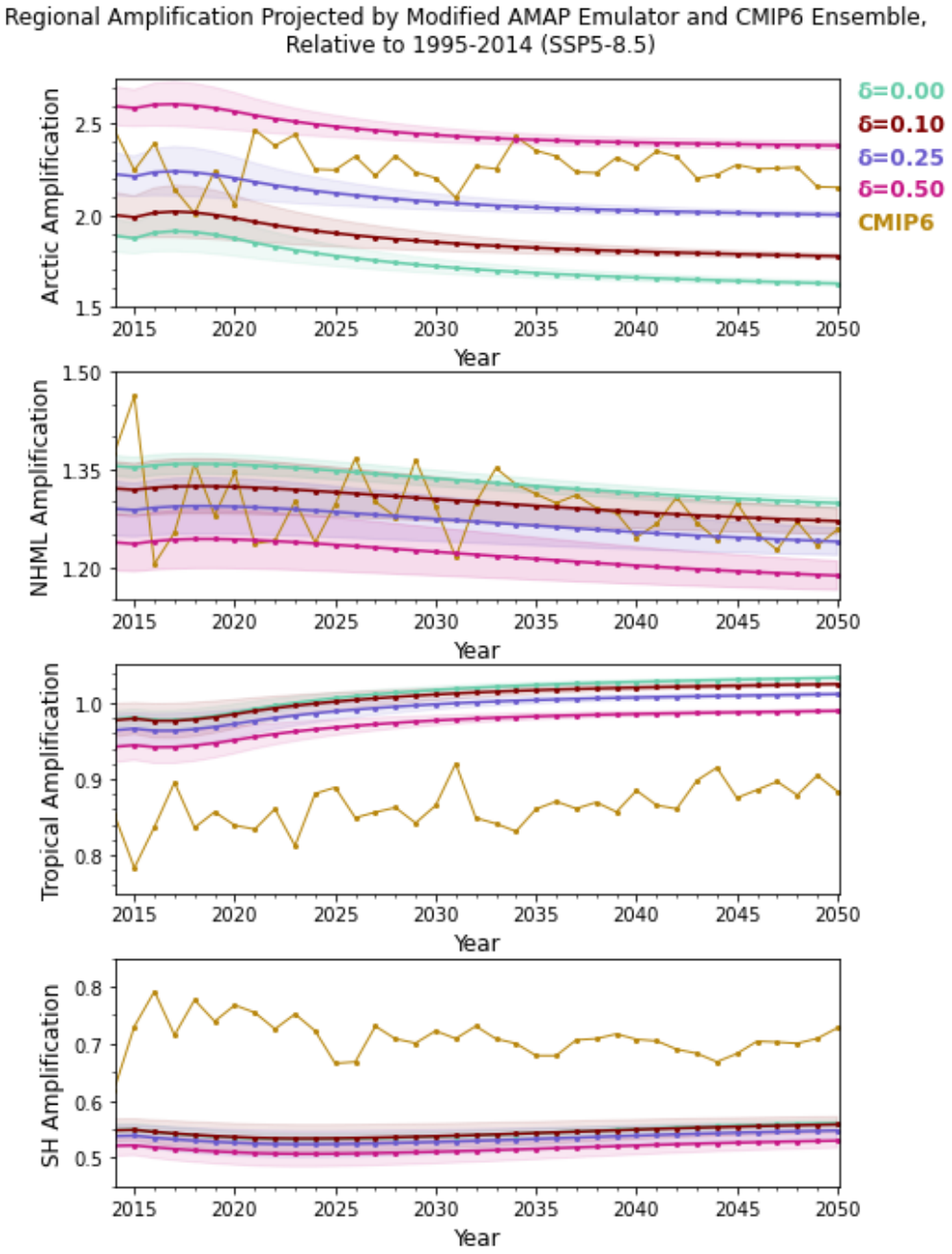

Figure 10: Regional amplification projected by the AMAP emulator for different δ settings, for SSP5-8.5. The uncertainty of these time series shown as filled in colour, and are standard deviation of the temperatures from the ensemble was taken as the temperature uncertainty for each year. This uncertainty was propagated with the uncertainty from the mean temperature over the reference period of 1995-2014. The corresponding results from the CMIP6 ensemble are shown for comparison, but error bars are neglected due to their large relative size. The uncertainties for these CMIP6 ensemble time series are shown in Figure 13 in Appendix C.

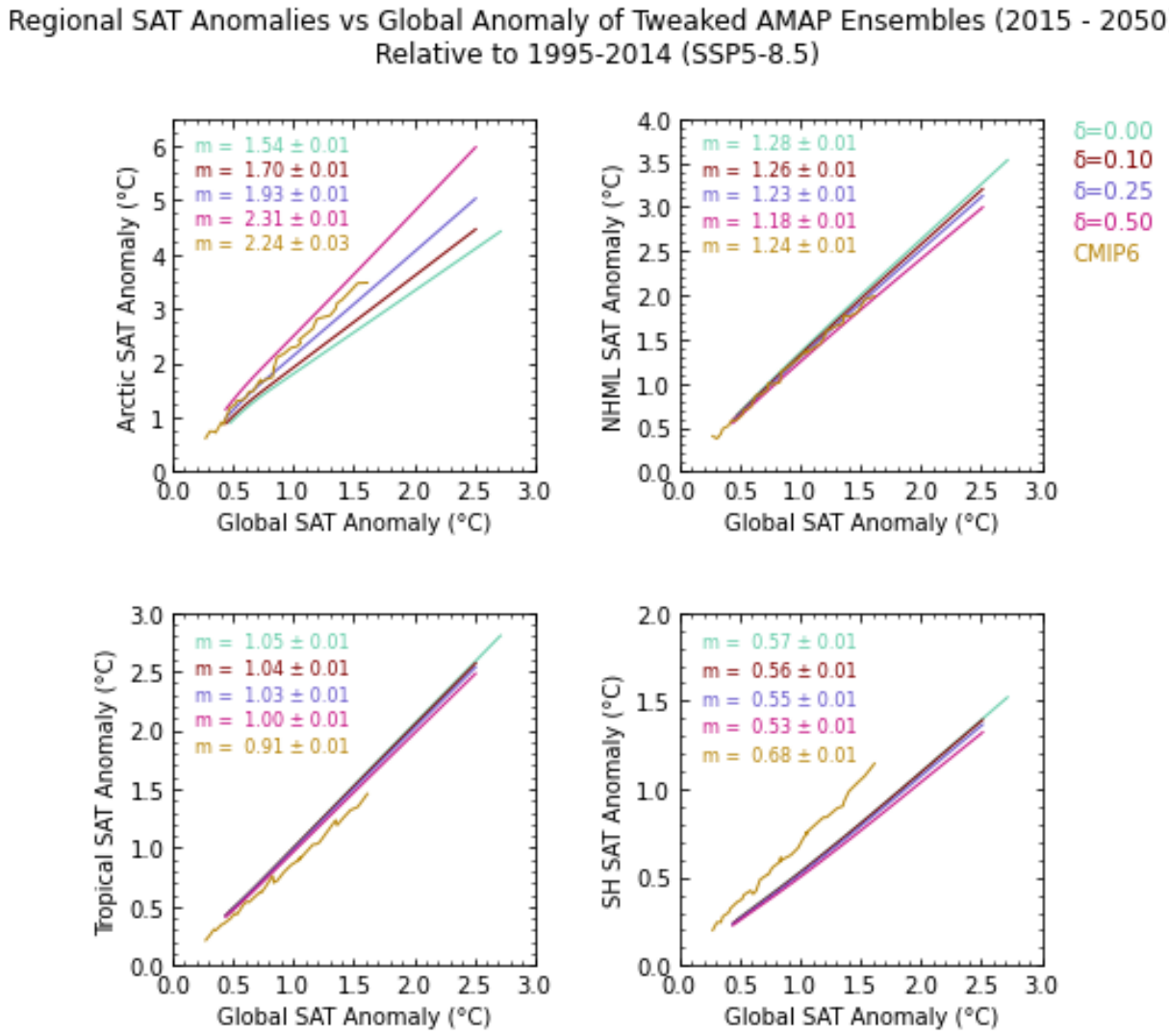

Figure 11: Results of RMA fitting of global versus regional SAT anomalies for four AMAP emulator tweakings, $\delta = \{0.00, 0.10, 0.25, 0.50\}$ and the large CMIP6 ensemble, for SSP5-8.5, along with the resulting slope m from the fits..

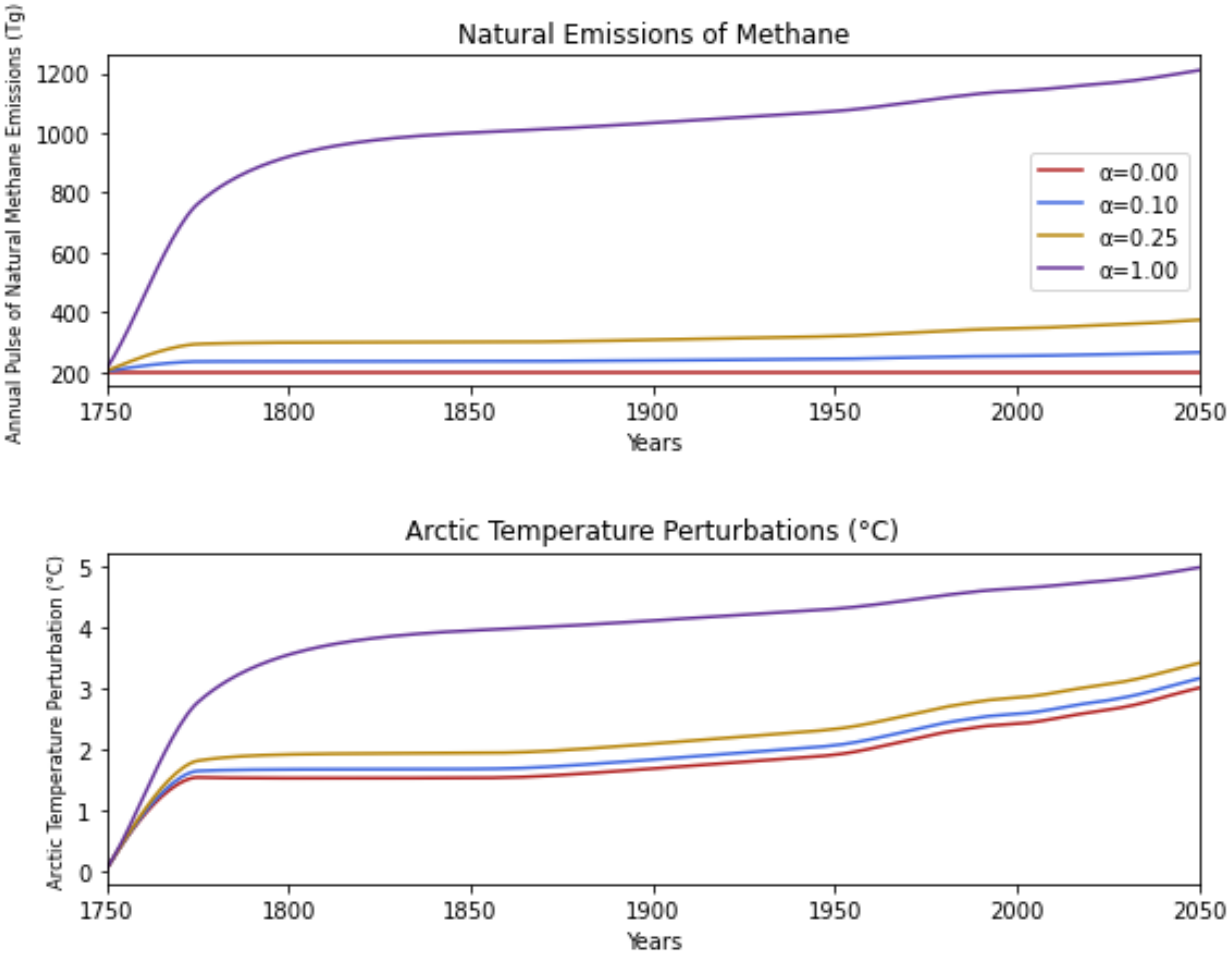

Figure 12: Natural emissions of CH_4 as a function of time and the Arctic temperature perturbations projected by the modified AMAP emulator, for SSP5-8.5.

The main objectives of this study included diagnosing the differences between the AMAP emulator and the most cutting edge ESMs, the modification of the AMAP emulator's RTP coefficients k_{lm} to better emulate Arctic temperatures, and adapting CH_4's representation in the emulator to include a positive feedback loop of natural CH_4 emissions and increases in Arctic temperature.

Through comparisons with two sets of CMIP6 results, the AMAP emulator was found to underestimate Arctic warming compared to one CMIP6 ensemble and overestimate Arctic warming compared to another. A common issue observed from these comparisons is that the amplification of Arctic warming relative to global warming is underestimated by the AMAP emulator. In an area-weighted rescaling of the RTP coefficients used by the AMAP emulator, it was found that an increase in RTP_{ARC} between 25% and 50% could be appropriate to better represent Arctic amplification. SSP5-8.5 Arctic temperature projections from a CMIP6 ensemble were found to generally lie between the results of the AMAP emulator modified with a 25% and 50% increased RTP_{ARC}. The ECS value was kept constant for this study, but it does have the potential to be changed, and could be beneficial for the emulator.

Results from implementing a simple positive feedback loop demonstrate the potential for an improved representation of CH_4 the AMAP emulator, but further investigation is required for a recommendation to be made.

For future endeavours, the RTP tweaking method used in this study could be extended to specify an increase or decrease to the RTP for the Northern Hemisphere midlatitudes, the tropics, and/or the Southern Hemisphere. In particular, the AMAP emulator was shown to greatly underestimate warming in the Southern Hemisphere and overestimate warming in the tropics. Additionally, the effects of this RTP tweaking can be studied for SSPs with lower radiative forcing than SSP5-8.5, which was the only the SSP included in this tweaking.

Further investigation into how natural emissions of CH_4 can also be conducted. Additionally, the CH_4 atmospheric lifetime can be updated. This could include modifying certain components or adding new factors to its atmospheric lifetime.

The limitations of the AMAP emulator can be further addressed and the model improved upon as it is used to study the impacts of short-lived climate forcers on Earth's climate.

References

1. K. von Salzen, “Technical Summary: The AMAP Climate and Air Quality Emulator,” 2021.

2. Z. R. J. Nicholls et al., “Reduced Complexity Model Intercomparison Project Phase 1: introduction and evaluation of global-mean temperature response,” Geosci. Model Dev., vol. 13, no. 11, pp. 5175–5190, 2020.

3. K. Kupiainen, M. Flanner, and S. Eckhardt, “Climate effects of other pollutants – short-lived climate forcers and the Arctic,” Global Arctic, pp. 171–187, 2022.

4. AMAP, Impacts of Short-lived Climate Forcers on Arctic Climate, Air Quality, and Human Health. Summary for Policy-makers. Tromsø, Norway: Arctic Monitoring and Assessment Programme (AMAP).

5. M. Previdi, K. L. Smith, and L. M. Polvani, “Arctic amplification of climate change: A review of underlying mechanisms,” Environmental Research Letters, vol. 16, no. 9, p. 093003, 2021.

6. K. von Salzen et al., “Clean air policies are key for successfully mitigating Arctic warming,” Earth Environment, 2022.

7. M. J. Prather, C. D. Holmes, and J. Hsu, “Reactive greenhouse gas scenarios: Systematic exploration of uncertainties and the role of atmospheric chemistry: ATMOSPHERIC CHEMISTRY AND GREENHOUSE GASES,” Geophys. Res. Lett., vol. 39, no. 9, 2012.

8. C. H. Whaley, R. Mahmood, K. von Salzen, B. Winter, S. Eckhardt, S. Arnold, S. Beagley, S. Becagli, R.-Y. Chien, J. Christensen, S. M. Damani, K. Eleftheriadis, N. Evangeliou, G. S. Faluvegi, M. Flanner, J. S. Fu, M. Gauss, F. Giardi, W. Gong, J. L. Hjorth, L. Huang, U. Im, Y. Kanaya, S. Krishnan, Z. Klimont, T. Kühn, J. Langner, K. S. Law, L. Marelle, A. Massling, D. Olivié, T. Onishi, N. Oshima, Y. Peng, D. A. Plummer, O. Popovicheva, L. Pozzoli, J.-C. Raut, M. Sand, L. N. Saunders, J. Schmale, S. Sharma, H. Skov, F. Taketani, M. A. Thomas, R. Traversi, K. Tsigaridis, S. Tsyro, S. Turnock, V. Vitale, K. A. Walker, M. Wang, D. Watson-Parris, and T. Weiss-Gibbons, “Model evaluation of short-lived climate forcers

for the Arctic Monitoring and Assessment Programme: A multi-species, multi-model study," Preprint. Gases/Atmospheric Modelling/Troposphere/Chemistry (chemical composition and reactions), Nov. 2021.

9. C. H. Whaley, R. Mahmood, K. von Salzen, B. Winter, S. Eckhardt, S. Arnold, S. Beagley, S. Becagli, R.-Y. Chien, J. Christensen, S. M. Damani, X. Dong, K. Eleftheriadis, N. Evangeliou, G. Faluvegi, M. Flanner, J. S. Fu, M. Gauss, F. Giardi, W. Gong, J. L. Hjorth, L. Huang, U. Im, Y. Kanaya, S. Krishnan, Z. Klimont, T. Kühn, J. Langner, K. S. Law, L. Marelle, A. Massling, D. Olivié, T. Onishi, N. Oshima, Y. Peng, D. A. Plummer, O. Popovicheva, L. Pozzoli, J.-C. Raut, M. Sand, L. N. Saunders, J. Schmale, S. Sharma, R. B. Skeie, H. Skov, F. Taketani, M. A. Thomas, R. Traversi, K. Tsigaridis, S. Tsyro, S. Turnock, V. Vitale, K. A. Walker, M. Wang, D. Watson-Parris, and T. Weiss-Gibbons, "Model evaluation of short-lived climate forcers for the Arctic Monitoring and Assessment Programme: A multi-species, multi-model study," Atmospheric Chemistry and Physics, vol. 22, no. 9, pp. 5775–5828, 2022.

10. A. Stohl et al., "Evaluating the climate and air quality impacts of short-lived pollutants," Atmos. Chem. Phys., vol. 15, no. 18, pp. 10529–10566, 2015.

11. D. M. Lawrence, C. D. Koven, S. C. Swenson, W. J. Riley, and A. G. Slater, "Permafrost thaw and resulting soil moisture changes regulate projected high-latitude co 2 and CH 4 emissions," Environmental Research Letters, vol. 10, no. 9, p. 094011, 2015.

12. https://www.ipcc.ch/report/ar6/wg1/chapter/chapter-6/.

13. I. S. A. Isaksen, M. Gauss, G. Myhre, K. M. Walter Anthony, and C. Ruppel, "Strong atmospheric chemistry feedback to climate warming from Arctic methane emissions: ARCTIC METHANE FEEDBACK," Global Biogeochem. Cycles, vol. 25, no. 2, 2011.

14. G. A. Meehl et al., "Context for interpreting equilibrium climate sensitivity and transient climate response from the CMIP6 Earth system models," Sci. Adv., vol. 6, no. 26, p. eaba1981, 2020.

15. J. Alcamo, M. Krol, and M. Posch, "An integrated analysis of sulfur emissions, acid deposition and climate change," Water Air Soil Pollut., vol. 85, no. 3, pp. 1539–1550, 1995.

16. D. Shindell and G. Faluvegi, "The net climate impact of coal-fired power plant emissions," Atmospheric Chemistry and Physics, vol. 10, no. 7, pp. 3247–3260, 2010.

17. G. A. Ban-Weiss, L. Cao, G. Bala, and K. Caldeira, "Dependence of climate forcing and response on the altitude of Black Carbon Aerosols," Climate Dynamics, vol. 38, no. 5-6, pp. 897–911, 2011.

18. World Health Organization, "Ambient air pollution: a global assessment of exposure and burden of disease," Clean Air J., vol. 26, no. 2, p. 6, 2016.

19. M. Brauer et al., "Exposure assessment for estimation of the global burden of disease attributable to outdoor air pollution," Environ. Sci. Technol., vol. 46, no. 2, pp. 652–660, 2012.

20. J. Lelieveld, J. S. Evans, M. Fnais, D. Giannadaki, and A. Pozzer, "The contribution of outdoor air pollution sources to premature mortality on a global scale," Nature, vol. 525, no. 7569, pp. 367–371, 2015.

21. R. J. Allen et al., "Significant climate benefits from near-term climate forcer mitigation in spite of aerosol reductions," Environ. Res. Lett., 2021.

22. J. Lelieveld, K. Klingmüller, A. Pozzer, R. T. Burnett, A. Haines, and V. Ramanathan, "Effects of fossil fuel and total anthropogenic emission removal on public health and climate," Proc. Natl. Acad. Sci. U. S. A., vol. 116, no. 15, pp. 7192–7197, 2019.

23. D. Shindell et al., "Simultaneously mitigating near-term climate change and improving human health and food security," Science, vol. 335, no. 6065, pp. 183–189, 2012.

24. M. D. Zelinka et al., "Causes of higher climate sensitivity in CMIP6 models," Geophys. Res. Lett., vol. 47, no. 1, 2020.

25. Z. Nicholls et al., "Reduced Complexity Model Intercomparison Project Phase 2: Synthesizing earth system knowledge for probabilistic climate projections," Earths Future, vol. 9, no. 6, p. e2020EF001900, 2021.

26. K. Riahi et al., "The Shared Socioeconomic Pathways and their energy, land use, and greenhouse gas emissions implications: An overview," Glob. Environ. Change, vol. 42, pp. 153–168, 2017.

27. M. Meinshausen, S. C. B. Raper, and T. M. L. Wigley, "Emulating coupled atmosphere-ocean and carbon cycle models with a simpler model, MAGICC6 – Part 1: Model description and calibration," Atmos. Chem. Phys., vol. 11, no. 4, pp. 1417–1456, 2011.

28. P. Good, J. M. Gregory, and J. A. Lowe, "A step-response simple climate model to reconstruct and interpret AOGCM projections: A STEP-RESPONSE SIMPLE CLIMATE MODEL," Geophys. Res. Lett., vol. 38, no. 1, 2011.

29. O. Geoffroy, D. Saint-Martin, D. J. L. Olivié, A. Voldoire, G. Bellon, and S. Tytéca, "Transient climate response in a two-layer energy-balance model. Part I: Analytical solution and parameter calibration using CMIP5 AOGCM experiments," J. Clim., vol. 26, no. 6, pp. 1841–1857, 2013.

30. P. M. Forster, A. C. Maycock, C. M. McKenna, and C. J. Smith, "Latest climate models confirm need for urgent mitigation," Nat. Clim. Chang., vol. 10, no. 1, pp. 7–10, 2020.

31. C. J. Smith et al., "FAIR v1.1: A simple emissions-based impulse response and carbon cycle model," 2017.

32. T. Gasser et al., "The compact Earth system model OSCAR v2.2: description and first results," Geosci. Model Dev., vol. 10, no. 1, pp. 271–319, 2017.

33. K. M. Foley, S. L. Napelenok, C. Jang, S. Phillips, B. J. Hubbell, and C. M. Fulcher, "Two reduced form air quality modeling techniques for rapidly calculating pollutant mitigation potential across many sources, locations and precursor emission types," Atmos. Environ. (1994), vol. 98, pp. 283–289, 2014.

34. J. Li et al., “A modeling study of source–receptor relationships in atmospheric particulate matter over Northeast Asia,” Atmos. Environ. (1994), vol. 91, pp. 40–51, 2014.

35. Y. Liu et al., “Source-receptor relationships for PM2.5 during typical pollution episodes in the Pearl River Delta city cluster, China,” Sci. Total Environ., vol. 596–597, pp. 194–206, 2017.

36. P. S. Porter, S. T. Rao, C. Hogrefe, and R. Mathur, “A reduced form model for ozone based on two decades of CMAQ simulations for the continental United States,” Atmos. Pollut. Res., vol. 8, no. 2, pp. 275–284, 2017.

37. R. Van Dingenen et al., “TM5-FASST: a global atmospheric source-receptor model for rapid impact analysis of emission changes on air quality and short-lived climate pollutants,” Atmos. Chem. Phys. Discuss., pp. 1–55, 2018.

38. J. Tsutsui, “Quantification of temperature response to CO2 forcing in atmosphere–ocean general circulation models,” Clim. Change, vol. 140, no. 2, pp. 287–305, 2017.

39. “About,” Amap.no. [Online]. Available: https://www.amap.no/about.

40. The Intergovernmental Panel on Climate Change (IPCC): 1990, Climate Change: The Intergovernmental Panel on Climate Change Scientific Assessment. Cambridge, UK: Cambridge University Press.

41. K. P. Shine, J. S. Fuglestvedt, K. Hailemariam, and N. Stuber, “Alternatives to the global warming potential for comparing climate impacts of emissions of greenhouse gases,” Clim. Change, vol. 68, no. 3, pp. 281–302, 2005.

42. O. Boucher and M. S. Reddy, “Climate trade-off between black carbon and carbon dioxide emissions,” Energy Policy, vol. 36, no. 1, pp. 193–200, 2008.

43. J. S. Fuglestvedt et al., “Transport impacts on atmosphere and climate: Metrics,” Atmos. Environ. (1994), vol. 44, no. 37, pp. 4648–4677, 2010.

44. D. Shindell and G. Faluvegi, “Climate response to regional radiative forcing during the twentieth century,” Nat. Geosci., vol. 2, no. 4, pp. 294–300, 2009.

45. D. T. Shindell, "Evaluation of the absolute regional temperature potential," Atmos. Chem. Phys., vol. 12, no. 17, pp. 7955–7960, 2012.

46. "Black carbon and ozone as Arctic climate forcers," Arctic Monitoring and Assessment Programme, 2015.

47. G. A. Schmidt et al., "Present-day atmospheric simulations using GISS ModelE: Comparison to in situ, satellite, and reanalysis data," J. Clim., vol. 19, no. 2, pp. 153–192, 2006.

48. F. J. M. M. Nijsse, P. M. Cox, and M. S. Williamson, "Emergent constraints on transient climate response (TCR) and equilibrium climate sensitivity (ECS) from historical warming in CMIP5 and CMIP6 models," Earth Syst. Dyn., vol. 11, no. 3, pp. 737–750, 2020.

49. S. Kirschke et al., "Three decades of global methane sources and sinks," Nat. Geosci., vol. 6, no. 10, pp. 813–823, 2013.

50. "Atmospheric chemistry and greenhouse gases," in The Scientific Basis. Contribution of Working Group I to the Third Assessment Report of the Intergovernmental Panel on Climate Change, 2001.

51. "Climate change 2013: The physical science basis," in Contribution of Working Group I to the fifth assessment report of the Intergovernmental Panel on Climate Change.

52. A. Voulgarakis et al., "Analysis of present day and future OH and methane lifetime in the ACCMIP simulations," Atmos. Chem. Phys., vol. 13, no. 5, pp. 2563–2587, 2013.

53. Z. Hausfather, K. Marvel, G. A. Schmidt, J. W. Nielsen-Gammon, and M. Zelinka, "Climate simulations: recognize the 'hot model' problem," Nature, vol. 605, no. 7908, pp. 26–29, 2022.

54. B. Kravitz et al., "Comparing surface and stratospheric impacts of geoengineering with different SO 2 injection strategies: Comparing surface and stratospheric impacts of geoengineering with different SO2 injection strategies," J. Geophys. Res., vol. 124, no. 14, pp. 7900–7918, 2019.

55. J. Ols, Friedmana, and A. J. Bohonakb, When are two pieces better than one: fitting and testing.

56. G. Vinetti, A. Taboni, and G. Ferretti, "A regression method for the power-duration relationship when both variables are subject to error," Eur. J. Appl. Physiol., vol. 120, no. 4, pp. 765–770, 2020.

57. K. Schwarzwald and N. Lenssen, "The importance of internal climate variability in climate impact projections," EarthArXiv, 2022.

58. M. Meinshausen et al., "The shared socio-economic pathway (SSP) greenhouse gas concentrations and their extensions to 2500," Geosci. Model Dev., vol. 13, no. 8, pp. 3571–3605, 2020.

APPENDIX A: Table of Models used from CMIP6

	SSP1-1.9	SSP1-2.6	SSP2-4.5	SSP3-7.0	SSP5-8.5
Models	FGOALS-g3 GFDL-ESM4 MIROC-ES2L MIROC6 MRI-ESM2-0	AWI-CM-1-1-MR BCC-CSM2-MR CMCC-CM2-SR5 FGOALS-f3-L FGOALS-g3 GFDL-ESM4 KIOST-ESM MIROC-ES2L MIROC6 MPI-ESM1-2-HR MPI-ESM1-2-LR MRI-ESM2-0 NorESM2-LM NorESM2-MM	ACCESS-ESM1-5 AWI-CM-1-1-MR BCC-CSM2-MR CMCC-CM2-SR5 FGOALS-f3-L FGOALS-g3 GFDL-CM4 GFDL-ESM4 KIOST-ESM MIROC-ES2L MIROC6 MPI-ESM1-2-HR MPI-ESM1-2-LR MRI-ESM2-0 NorESM2-LM NorESM2-MM	AWI-CM-1-1-MR BCC-CSM2-MR CMCC-CM2-SR5 FGOALS-f3-L FGOALS-g3 GFDL-ESM4 MIROC-ES2L MIROC6 MPI-ESM1-2-HR MPI-ESM1-2-LR MRI-ESM2-0 NorESM2-LM NorESM2-MM	AWI-CM-1-1-MR BCC-CSM2-MR CMCC-CM2-SR5 FGOALS-f3-L FGOALS-g3 GFDL-CM4 GFDL-ESM4 KIOST-ESM MIROC-ES2L MIROC6 MPI-ESM1-2-HR MPI-ESM1-2-LR MRI-ESM2-0 NorESM2-LM NorESM2-MM
Total Number of Models	5	14	16	13	15

Table 6: Climate models included in the CMIP6 ensemble for each of the SSPs shown in Figures 3 and 4.

APPENDIX B: Tweaked RTP Coefficients

		l							
		$\delta = 0.00$				$\delta = 0.10$			
		Arctic	NHML	Tropics	SH	Arctic	NHML	Tropics	SH
m	Arctic	0.31	0.17	0.16	0.06	0.341	0.187	0.176	0.066
	NHML	0.06	0.24	0.17	0.07	0.055	0.238	0.168	0.069
	Tropics	0.02	0.10	0.24	0.09	0.018	0.099	0.239	0.089
	SH	0.00	0.02	0.05	0.19	0.000	0.0186	0.049	0.189

		l							
		$\delta = 0.25$				$\delta = 0.50$			
		Arctic	NHML	Tropics	SH	Arctic	NHML	Tropics	SH
m	Arctic	0.388	0.213	0.200	0.075	0.465	0.255	0.240	0.09
	NHML	0.047	0.235	0.165	0.068	0.034	0.230	0.161	0.067
	Tropics	0.014	0.098	0.238	0.089	0.009	0.096	0.236	0.089
	SH	0.000	0.016	0.047	0.189	0.000	0.013	0.043	0.187

Table 7: RTP coefficients k_{lm} for an AMAP emulator settings of $\delta \in \{ 0.00, 0.10, 0.25, 0.50\}$, rounded to 3 significant figures for the modified coefficient versions. The default coefficients ($\delta = 0.00$) are shown with two decimal places because that is the default setting of the emulator.

APPENDIX C: Additional Figures

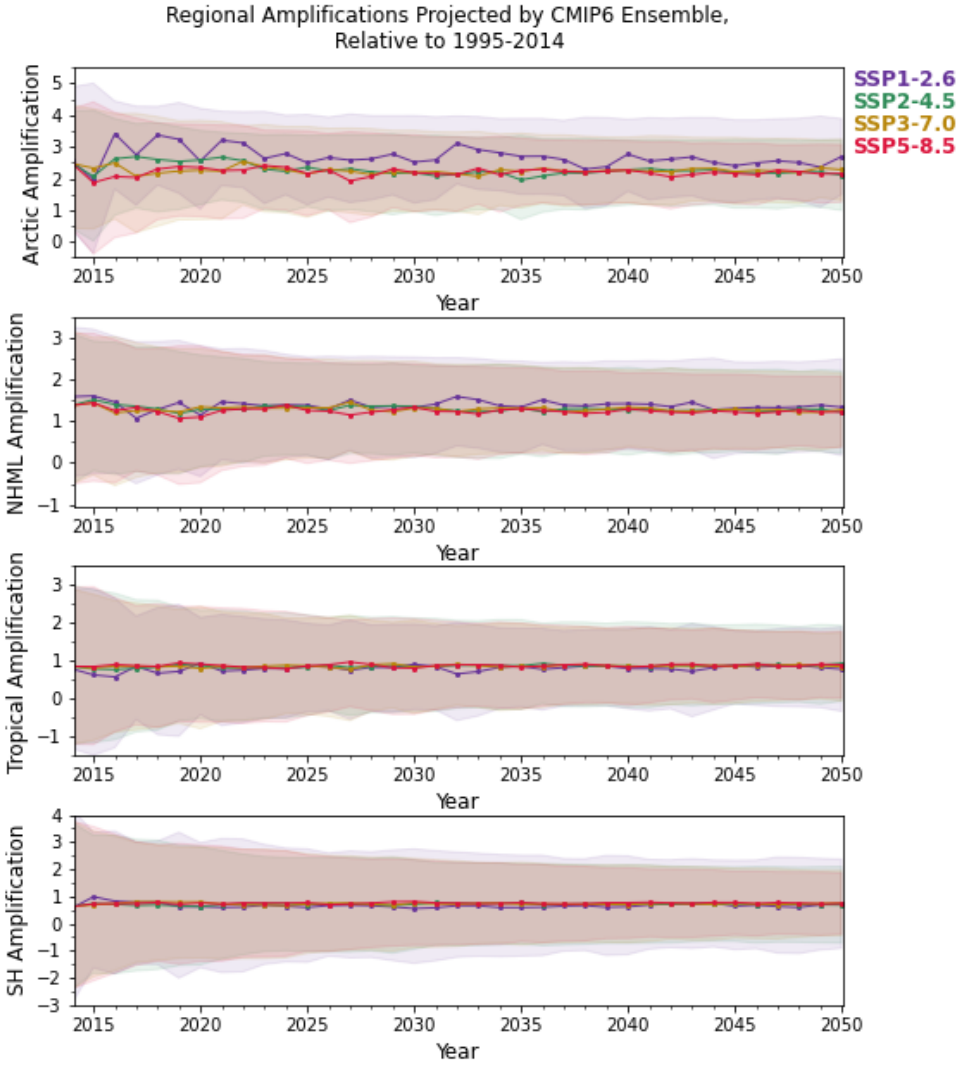

Figure 13: Same as Figure 6, but with added error bars shown through shaded colour for each of the SSPs. The standard deviation of the temperatures from the ensemble was taken as the temperature uncertainty for each year. The error bars are the propagated uncertainty of the two mean SAT anomalies in the dividend (regional and global).

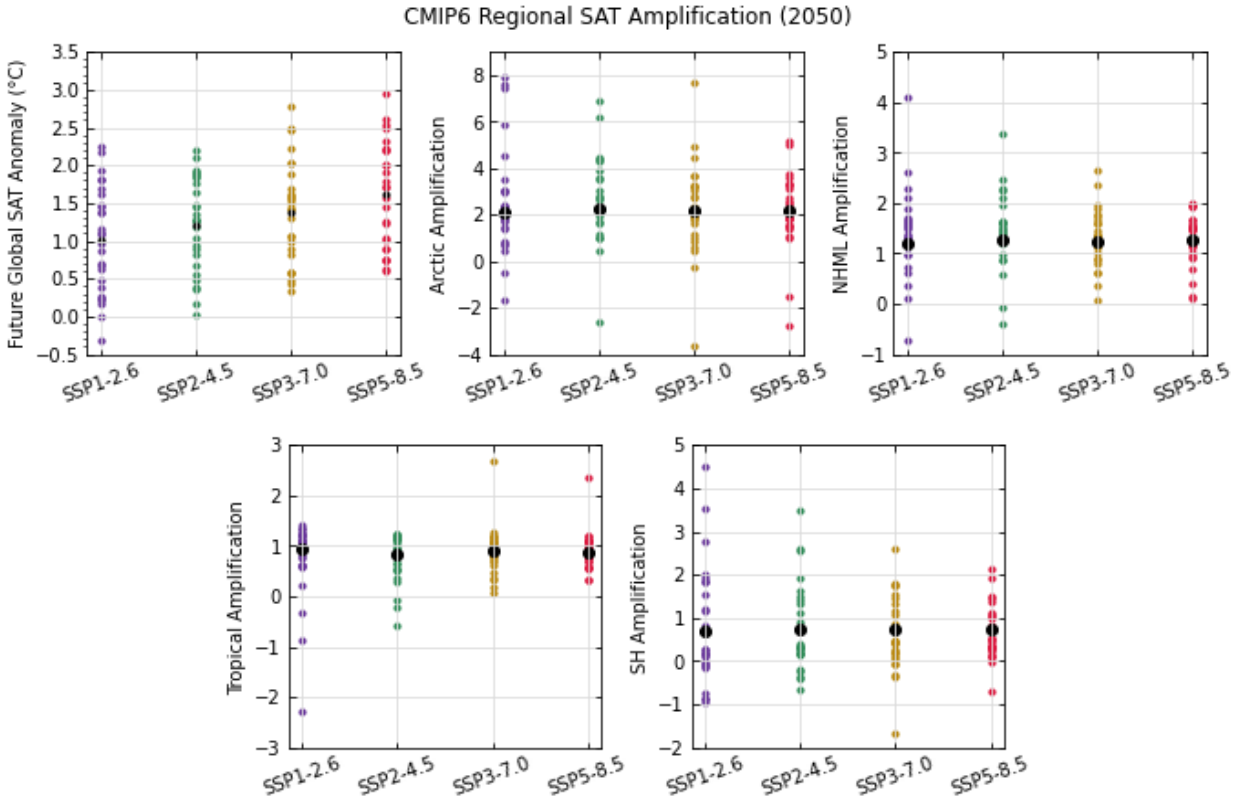

Figure 14: Global surface temperature anomalies relative to 1995-2014 projected for 2050 by CMIP6 ensemble and regional amplifications for the Arctic, Northern Hemisphere midlatitudes, the tropics, and the Southern Hemisphere in the year Amplification. For each of the four SSPs, the coloured points represent the global anomaly from an individual realization from the CMIP6 ensemble (upper left) or the ratio of a regional surface temperature anomaly to the global anomaly for a particular region (upper middle and right, bottom). The black bullets represent the ensemble average regional surface temperature anomaly divided by the ensemble global surface temperature anomaly for 2050.

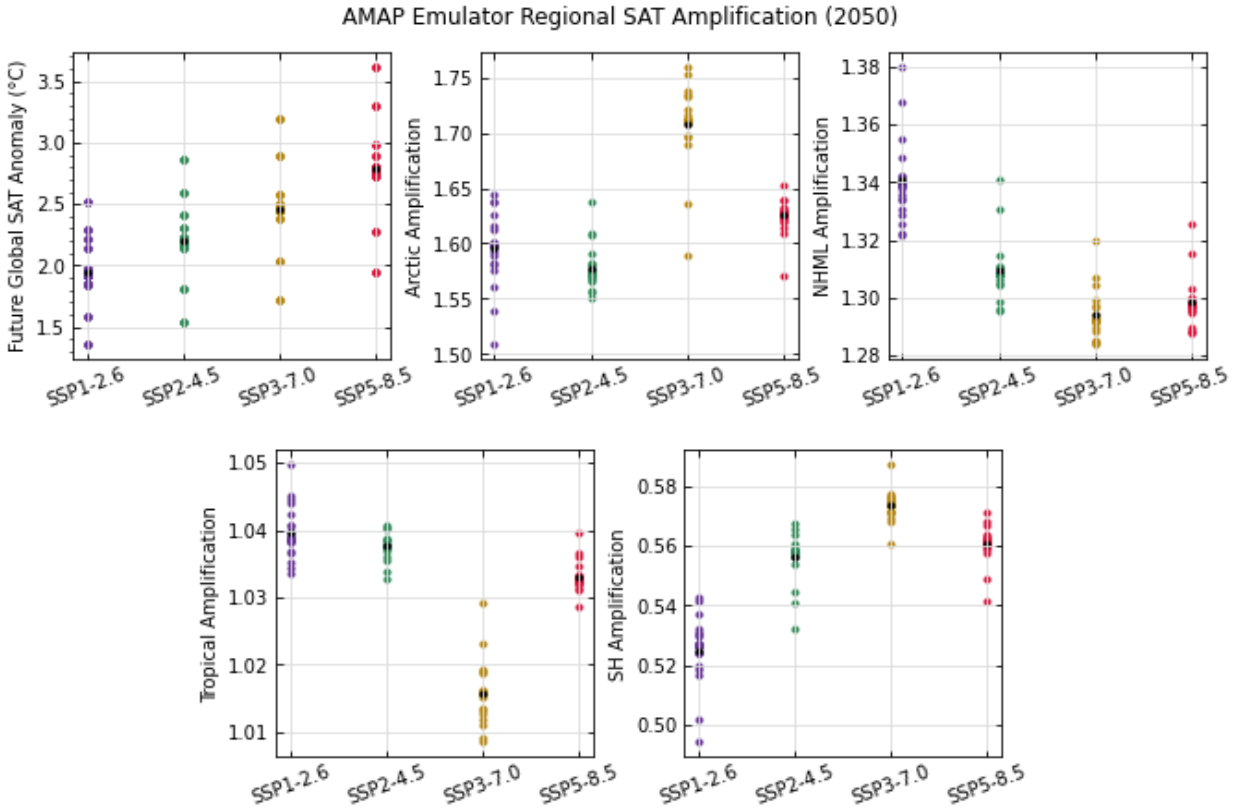

Figure 15: Same as Figure 14, but for an ensemble of 24 realizations of AMAP emulator on its default settings ($\delta = 0.00$).

APPENDIX D: Tabulated Regional Amplifications

		Arctic	NHML	Tropics	SH
2030	CMIP6	2.20 ±1.47	1.29 1.20	0.87 ±1.30	0.72 ±2.31
	AMAP$_{\delta=0.00}$	1.83 ±0.06	1.35 ±0.01	1.00 ±0.01	0.54 ±0.01
	AMAP$_{\delta=0.10}$	1.96 ±0.06	1.33 ±0.01	0.99 ±0.01	0.53 ±0.01
	AMAP$_{\delta=0.25}$	2.18 ±0.06	1.30 ±0.01	0.98 ±0.01	0.52 ±0.01
2050	CMIP6	2.15 ±0.75	1.26 0.66	0.88 ±0.66	0.73 ±1.11
	AMAP$_{\delta=0.00}$	1.74 ±0.09	1.33 ±0.02	1.01 ±0.02	0.54 ±0.01
	AMAP$_{\delta=0.10}$	1.87 ±0.09	1.31 ±0.02	1.01 ±0.02	0.54 ±0.01
	AMAP$_{\delta=0.25}$	2.09 ±0.08	1.28 ±0.02	0.99 ±0.02	0.53 ±0.01
	AMAP$_{\delta=0.50}$	2.46 ±0.08	1.23 ±0.02	0.97 ±0.02	0.51 ±0.01

Table 8: This table presents the regional amplifications, taken as the average regional surface air temperature anomaly to the global anomaly. for SSP5-8.5 for the large CMIP6 ensemble at the AMAP emulator in its default setting (AMAP$_{\delta=0.00}$) and tweaked settings (AMAP$_{\delta=0.10}$, AMAP$_{\delta=0.25}$, AMAP$_{\delta=0.50}$). The regional amplifications are shown for the years 2030 and 2050.